DNA Repair 63 (2018) 25–38

Contents lists available at ScienceDirect

DNA Repair

journal homepage: www.elsevier.com/locate/dnarepair

Repair of exogenous DNA double-strand breaks promotes chromosome synapsis in SPO11-mutant mouse meiocytes, and is altered in the absence of HORMAD1

Fabrizia Carofiglio[a], Esther Sleddens-Linkels[a], Evelyne Wassenaar[a], Akiko Inagaki[a,1], Wiggert A. van Cappellen[b], J. Anton Grootegoed[a], Attila Toth[c], Willy M. Baarends[a,*]

[a] Department of Developmental Biology, Erasmus MC – University Medical Center, Rotterdam, The Netherlands
[b] Erasmus Optical Imaging Centre, Department of Pathology, Erasmus MC – University Medical Center, Rotterdam, The Netherlands
[c] Molecular Cell Biology Group/Experimental Center, Institute of Physiological Chemistry Medical School, MTZ, Dresden University of Technology, Dresden, Germany

ARTICLE INFO

Keywords:
Meiosis
SPO11
Homologous recombination
DMC1
RAD51
HORMAD1

ABSTRACT

Repair of SPO11-dependent DNA double-strand breaks (DSBs) via homologous recombination (HR) is essential for stable homologous chromosome pairing and synapsis during meiotic prophase. Here, we induced radiation-induced DSBs to study meiotic recombination and homologous chromosome pairing in mouse meiocytes in the absence of SPO11 activity (*Spo11*$^{YF/YF}$ model), and in the absence of both SPO11 and HORMAD1 (*Spo11/Hormad1* dko). Within 30 min after 5 Gy irradiation of *Spo11*$^{YF/YF}$ mice, 140–160 DSB repair foci were detected, which specifically localized to the synaptonemal complex axes. Repair of radiation-induced DSBs was incomplete in *Spo11*$^{YF/YF}$ compared to *Spo11*$^{+/YF}$ meiocytes. Still, repair of exogenous DSBs promoted partial recovery of chromosome pairing and synapsis in *Spo11*$^{YF/YF}$ meiocytes. This indicates that at least part of the exogenous DSBs can be processed in an interhomolog recombination repair pathway. Interestingly, in a seperate experiment, using 3 Gy of irradiation, we observed that *Spo11/Hormad1* dko spermatocytes contained fewer remaining DSB repair foci at 48 h after irradiation compared to irradiated *Spo11* knockout spermatocytes. Together, these results show that recruitment of exogenous DSBs to the synaptonemal complex, in conjunction with repair of exogenous DSBs via the homologous chromosome, contributes to homology recognition. In addition, the data suggest a role for HORMAD1 in DNA repair pathway choice in mouse meiocytes.

1. Introduction

Meiosis allows generation of haploid gametes from diploid precursor cells. In the first meiotic division, recombination and segregation of homologous chromosomes takes place, whereas sister chromatids are separated in the second division. At the onset of meiotic prophase I, more than 200 meiotically regulated DNA double-strand breaks (DSBs) are induced by the SPO11/TOPOVIBL complex in the mouse [1–4]. Essential components of non-homologous end joining (NHEJ), an error-prone DSB repair mechanism, are suppressed in early meiotic prophase of mouse spermatocytes [5], and meiotic DSBs are thought to be repaired via homologous recombination (HR), although a contribution of pathways such as alternative NHEJ or single-strand annealing cannot be excluded [6,7]. HR repair is mediated by recombinases, proteins that have DNA-dependent ATPase activity and form filaments on the single-stranded resected DNA ends at DSB sites. In meiotic cells, two recombinases are expressed: RAD51 and DMC1. RAD51 is known to be essential for homologous recombination repair in mitotic cells [8,9], and is thought to perform an accessory function in mouse meiosis, in analogy to what has been described for yeast RAD51 [10]. Recent knockdown experiments indeed indicate a role for RAD51 in meiotic recombination and crossover formation [11]. DMC1 has indispensable meiosis-specific activity [12,13]. Repair via homologous recombination implies the use of an intact DNA template to recover the missing genetic information. In meiotic prophase I cells, three templates can be used: the sister chromatid, that is tethered to its counterpart by (meiosis-specific) cohesins which are loaded during [14,15] and after [16–18] pre-meiotic S phase, and either one of the two chromatids of the homologous chromosome. For meiosis in *S. cerevisiae*, it was shown that the homologous chromosome is preferably used as a meiotic recombination partner, a phenomenon that is named interhomolog bias [19]. This condition requires several proteins which are associated with

* Corresponding author.
E-mail address: w.baarends@erasmusmc.nl (W.M. Baarends).
[1] Current address: Laboratory of Chromosome Biology, Memorial Sloan Kettering Cancer Center, New York, USA.

https://doi.org/10.1016/j.dnarep.2018.01.007
Received 22 August 2017; Received in revised form 16 January 2018; Accepted 17 January 2018
Available online 31 January 2018

the synaptonemal complex scaffold (Hop1, Red1, Hed1, Rec8, Mek1), or function in the homologous recombination pathway (Rad51, Dmc1) [20]. In mouse, no direct evidence of interhomolog bias has been provided so far. However, in spermatocytes, several DSB repair foci are present on the unsynapsed arm of the X chromosome, that only has the sister chromatid available as repair template, long after autosomal breaks have been fully repaired [21,22]. Recent data led to the suggestion that new DSBs are induced on chromatin areas that fail to synapse [23–25]. However, it is likely that X chromosome-associated foci in pachytene represent (in part) persistent unrepaired DSBs, because the key DSB promoting SPO11 auxilliary proteins IHO1 [26] and MEI4 [27] are both depleted from the unsynapsed sex chromosomes in early pachytene, indicating cessation of DSB formation upon pachytene initiation. Therefore, the persistense of unrepaired DSB markers on sex chromosomes indicates that the sister chromatid is not used efficiently as a template for the completion of repair, at least till late pachytene. Based on this observation, and the observation of persisting repair foci in meiocytes of DSB repair and synaptonemal complex mutants [28–35] such an interhomolog bias is expected to be operational on mouse autosomes as well. This would imply that the majority of mouse meiotic DSBs is repaired via homologous recombination using one of the chromatids of the homologous chromosome, rather than the sister chromatid, as a template. As an important consequence, recombinational DSB repair can promote homology recognition, juxtaposition of pairing chromosomes, and finally synapsis. This is established by the accumulation of central and transverse element proteins of the synaptonemal complex, such as SYCP1, TEX12, SYCE2, and SYCE3 [36–39]. These synaptonemal complex components zip together the lateral elements (composed of SYCP2 and SYCP3 complexes) that form along the bases of the chromatin loops of each chromosome [40,41].

In the absence of SPO11-induced meiotic DSBs, axial elements still form, but homologous pairing and synapsis are severely impaired in mouse meiocytes; some heterologous synapsis can occur, but both spermatocytes and oocytes do not proceed beyond a zygotene-like stage [1,3,42].

In a yeast strain carrying a *spo11* mutation, partial rescue of the meiotic defect was achieved by X-irradiation, with a six-fold increase of spore viability, showing that exogenous DNA lesions can partially substitute for Spo11-activity [43]. Similarly, improved centromeric interactions have been observed in *Spo11* knockout spermatocytes upon cisplatin treatment [3].

Herein, we aimed to study the role of meiotic HR repair in favouring homologous chromosome synapsis in mouse. First, we investigated if meiosis-specific processing of DSBs depends on SPO11-mediated formation of these breaks. Second, we determined whether processing of radiation-induced DSBs can contribute to homology recognition and synapsis. Finally, we addressed if the processing of exogenous DSBs on a *Spo11* knockout background is affected by absence of HORMAD1, which is a protein that might be involved in the enforcement of interhomolog bias in mammals [25,44]. To prevent endogenous DSB formation, we used mice carrying a SPO11 amino acid replacement (Y138F, hereafter referred to as $Spo11^{YF/YF}$), which abrogates the enzymatic activity of SPO11 and results in a synapsis-deficient phenotype [42], as well a $Spo11^{-/-}$ mice, that display a very similar phenotype [1]. We generated exogenous DSBs by γ-irradiation of leptotene meiocytes. When we studied the early processing of the radiation-induced DSBs, we observed that the DNA repair foci were specifically localized on the axial elements. Irradiation is expected to generate DSBs randomly in the genome, therefore this observation indicates relocalization of DSBs to the chromosomal axes. Subsequently, we analysed the dynamics of exogenous DSB repair in $Spo11^{YF/YF}$ spermatocytes and oocytes, compared to $Spo11^{+/YF}$ controls. We observed that many exogenous DSBs persisted for at least several days in homozygous *Spo11* mutant meiocytes, although the machinery to repair DSBs by HR is intact in both $Spo11^{YF/YF}$ and $Spo11^{+/YF}$ meiocytes, and the sister chromatid is theoretically available as template for repair. This result indicates that repair of exogenous breaks as it occurs in somatic cells is inhibited. This might indicate that the interhomolog bias is imposed on these DSBs, and intersister interactions are destabilized or inhibited. As expected based on this notion, homologous chromosome pairing and synapsis on the $Spo11^{YF/YF}$ mutant background were partially rescued by the irradiation treatment, suggesting that the subpopulation of breaks that is repaired via the homolog contributes to the establishment of interhomolog interactions. Finally we studied the effect of a *Hormad1* null mutation [45] on the processing of exogenous DSBs on a $Spo11^{-/-}$ background. We observed altered processing of repair foci in spermatocytes at 48 h after irradiation in the double knockout compared to the single *Spo11* knockout. Taken together, our data show that exogenous DSBs recruit the meiosis-specific HR repair machinery, are translocated to the axial elements, contribute to homology recognition, and that their repair is modulated by HORMAD1.

2. Results

2.1. Radiation-induced DSBs rapidly localize on the synaptonemal complex

We treated $Spo11^{+/YF}$ and $Spo11^{YF/YF}$ adult male mice with γ-irradiation, at a dose of 5 Gy, and analysed DSB markers in leptotene spermatocytes isolated from mice sacrificed 30 and 60 min after irradiation.

Replication protein A (RPA) specifically binds to single-stranded DNA [46–48] and it forms foci in meiotic cells as soon as meiotic DSBs are resected [42,49]. We observed RPA foci in irradiated $Spo11^{YF/YF}$ leptotene spermatocytes by 30 min after irradiation (Fig. 1A and B). In a previous study, we reported that RPA foci are almost completely absent in non-irradiated spermatocytes and oocytes from $Spo11^{YF/YF}$ mice ([42], and Fig. 1A); therefore, we deduced that we could refer to RPA foci as a proxy of radiation-induced DSBs. Radiation-induced DSBs are expected to be randomly distributed in the nucleus, and to elicit repair foci formation without specific localization. Interestingly, we observed that RPA foci, although scattered around the nuclear volume, were preferentially associated with the axial elements, although the percentage of foci that colocalised with SYCP3 axes was slightly lower in the irradiated samples compared to the unirradiated control. (Fig. 1A, close-ups, and quantitatively assessed in Fig. 1C). In $Spo11^{YF/YF}$ spermatocytes, the maximum number of foci (167 ± 30, Table 1) was reached 30 min after irradiation, and only 6 foci were observed in the non-irradiated nuclei, which indicates that around 160 DSBs were induced. In irradiated $Spo11^{+/YF}$ spermatocytes, 263 ± 58 RPA foci were observed, which was 127 more than in the unirradiated control (136 ± 37 RPA foci), and accumulation occurred with slower kinetics compared to the $Spo11^{YF/YF}$ spermatocytes (Fig. 1B, Table 1). These differences may indicate that more time is required to process the radiation-induced DSBs in $Spo11^{+/YF}$ compared to $Spo11^{YF/YF}$ spermatocytes, perhaps due to limiting amounts of the involved proteins. In addition, on the $Spo11^{+/YF}$ background, we cannot exclude that the number of endogenously induced DSB foci (by SPO11) is reduced upon irradiation, when factors become more limiting. In mouse meiotic prophase, ATM restrains SPO11 activity via a negative feedback loop [50], to limit the number of meiotic DSBs. If exogenous DSBs contribute to the activation of such a feedback response, this could reduce the number of SPO11-dependent DSBs that are actually formed in irradiated $Spo11^{+/YF}$ spermatocytes. Thus, limiting amounts of RPA, or of proteins that recruit RPA, as well as reduction of SPO11 activity might lead to underestimation of the number of exogenously induced DSBs on this background.

During meiotic prophase I in wild type meiocytes, RAD51 and its meiosis-specific homolog DMC1 are recruited to SPO11-dependent DSBs [51–53]. These two recombinases have been shown to mostly colocalize in DSB repair foci [53]. We observed similar patterns of accumulation using RAD51 and DMC1 antibodies in $Spo11^{YF/YF}$ leptotene spermatocytes after irradiation (Fig. 2A and B), indicating that both

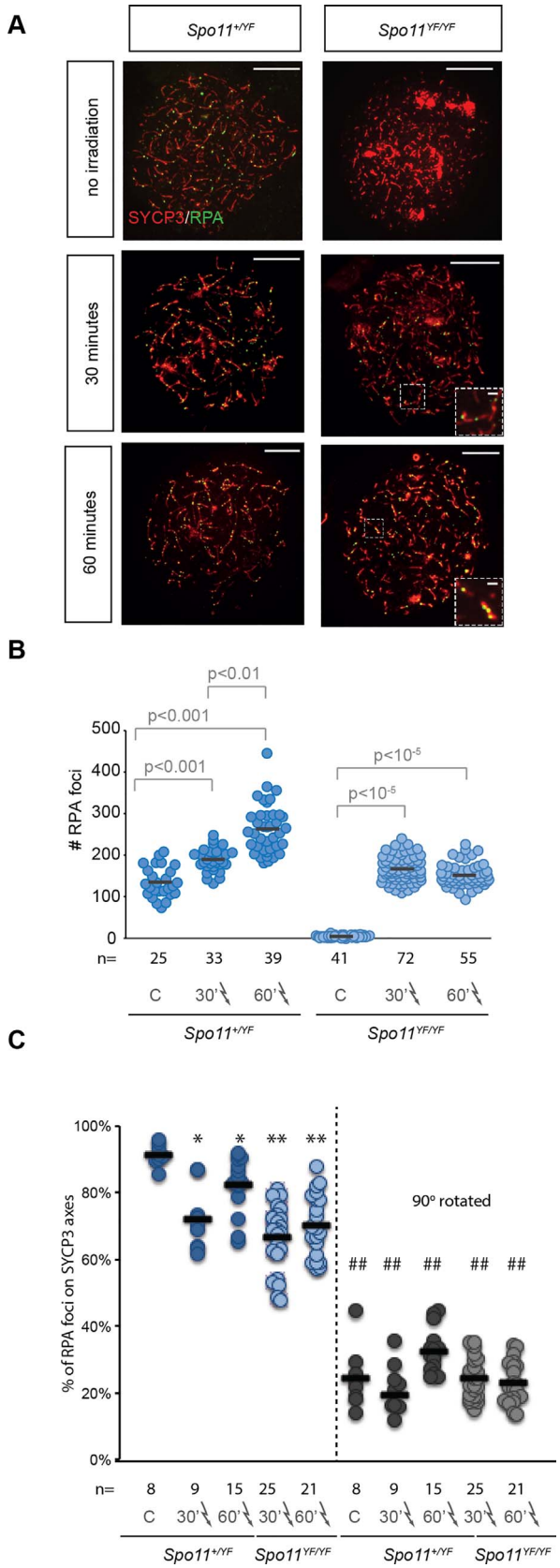

Fig 1. RPA protein foci upon irradiation of *Spo11*$^{+/YF}$ and *Spo11*$^{YF/YF}$ spermatocytes.
(A) Co-staining of RPA (green) and SYCP3 (red) in irradiated *Spo11*$^{+/YF}$ (left panel) and *Spo11*$^{YF/YF}$ (right panel) leptotene spermatocyte nuclei, 30 (left panels) and 60 (right panels) minutes after irradiation, and in non-irradiated controls. In the absence of irradiation, very few RPA foci can be detected in *Spo11*$^{YF/YF}$ leptotene spermatocytes, whereas numerous RPA foci have formed in leptotene spermatocytes, of which the vast majority colocalizes with the chromosomal axes. At both timepoints after irradiation, most RPA foci were found in association with the chromosomal axes in both genotypes; the close-ups show representative areas of the nucleus. Scale bar represents 10 μm in pictures of whole nuclei, and 1 μm in close-ups.
(B) The number of RPA foci was counted in *Spo11*$^{+/YF}$ and *Spo11*$^{YF/YF}$ leptotene spermatocytes, in control nuclei (C = non-irradiated), and at 30 and 60 min after irradiation. Statistically significant differences are marked in the plot (Mann-Whitney U). Each individual measurement is shown. horizontal lines indicate average values. n indicates the number of nuclei analysed for each genotype and condition.
(C) The percentage of RPA foci colocalising with SYCP3 was analysed in *Spo11*$^{+/YF}$ and *Spo11*$^{YF/YF}$ leptotene spermatocytes, in control nuclei (C = non-irradiated), and at 30 and 60 min after irradiation. Lines indicate average values. All true images were significantly different from their corresponding rotated images (## $p < 0.001$ Mann-Whitney U), and significant differences between non irradiated *Spo11*$^{+/YF}$ and other groups are indicated by * ($p < 0.05$) or ** ($p < 0.001$). n indicates the number of nuclei analysed for each genotype and condition. (For interpretation of the references to colour in this figure legend, the reader is referred to the web version of this article.)

RAD51 and DMC1 are recruited to the exogenous DSBs to form repair foci. It should be noted that we cannot formally exclude that the polyclonal RAD51 antibody may also recognize DMC1 to some extent, but the monoclonal DMC1 antibody does not cross-react with RAD51. Furthermore, colocalisation of the two proteins is not 100% indicating that some repair foci contain a detectable amount of only one of the two recombinases, making crossreaction unlikely (compare RAD51 to DMC1 in enlargements in Fig. 2B). Our observations are coherent with previous studies in which we showed that γ-irradiation results in formation of additional RAD51/DMC1 foci in wild type leptotene spermatocytes [54,55]. Similar to what we observed for RPA, the majority of RAD51/DMC1 foci were specifically associated with the axial elements (Fig. 2A and B, Supplemental Fig. 1A and B), confirming that the damage-induced DSBs are tethered to the axes before presynaptic recombinase filaments can be formed. In addition, the dynamics of RPA versus RAD51/DMC1 accumulation are consistent with a model in which RPA accumulates first, and is subsequently replaced by RAD51 and DMC1, as suggested previously [56].

In *Spo11*$^{YF/YF}$ leptotene spermatocyte nuclei, the number of RAD51 and DMC1 foci both increased from an average of 6 and 5 in non-irradiated nuclei (Fig. 2C, [42]) to a maximum of 150 ± 40 and 143 ± 45 at 60 min following irradiation, respectively (Fig. 2C, Table 1). This would indicate that around 140 exogenous DSBs can be visualized by RAD51/DMC1 immunostaining upon irradiation. This is a bit less than what we observed for RPA, which could be due to differences in signal-to-noise ratio between immunostaining of the different proteins, or might be related to differences in life-time of RPA and RAD51/DMC1 foci.

In *Spo11*$^{+/YF}$ and *Spo11*$^{YF/YF}$ leptotene nuclei, it is expected that the same number of DSBs is induced by the same radiation dose. However, the maximum increase in the numbers of RAD51 and DMC1 foci in irradiated *Spo11*$^{+/YF}$ leptotene spermatocytes was only 56 for DMC1 and 84 for RAD51 (Table 1). This indicates that RAD51 and DMC1 foci formation on radiation-induced breaks on the *Spo11*$^{+/YF}$ background is much less efficient, compared to what is observed on the *Spo11*$^{YF/YF}$ background, and also compared to what was observed for RPA. Although there may be technical issues associated with the efficiency of antigen detection by each antibody, this indicates that the recombinases RAD51 and DMC1 might become limiting when extra DSBs are induced.

2.2. Radiation-induced DSBs stimulate synapsis in *Spo11*$^{YF/YF}$ spermatocytes and oocytes

Given that radiation induced recombination foci associate with axial elements, we wondered if these axis-associated radiation-induced DSBs also promote juxtaposition of homologous chromosome axes and

Table 1
Protein foci formation shortly after 5 Gy irradiation in *Spo11*$^{+/YF}$ and *Spo11*$^{YF/YF}$ leptotene spermatocytes (averages ± standard deviation; n > 60).

	genotype	protein foci		time after irradiation			
			control[a]	30 min		60 min	
				total	induced	total	induced
Spermatocytes	*Spo11*$^{+/YF}$	RPA	136 ± 37	190 ± 26	54	263 ± 58	127
		RAD51	138 ± 27[b]	137 ± 20	ns	222 ± 54	84
		DMC1	93 ± 35	114 ± 20	ns	149 ± 64	56
	Spo11$^{YF/YF}$	RPA	6 ± 3[b]	167 ± 30	161	152 ± 27	146
		RAD51	6 ± 3[b]	128 ± 32	122	150 ± 40	144
		DMC1	5 ± 3[b]	115 ± 39	110	143 ± 45	138

[a] control was not irradiated.
[b] data from [42].

synaptonemal complex formation. To address this, we analysed the effect of DSBs induced by radiation during leptotene on the progression of chromosome pairing and synapsis as spermatocytes developed further. A time period of 48 h and 120 h is required for the transition from leptotene to late zygotene and to midpachytene, respectively. Thus, male mice were sacrificed at 48 h or 120 h following 5 Gy irradiation (Fig. 3A). A dose of 5 Gy will kill most of the spermatogonia and preleptotene spermatocytes, but more than half of the spermatocytes at later stages will survive, and progress through meiotic prophase with normal timing of subsequent events [57]. Thus, the late zygotene and midpachytene (like) spermatocytes analysed at the chosen timepoints will have developed from cells that were at the leptotene stage at the time of irradiation. To analyse the effect of radiation-induced DSBs on synapsis in *Spo11*$^{YF/YF}$ oocytes, we followed a different experimental time schedule, coherent with the timing of female meiotic prophase, which is initiated during embryonic development. Pregnant *Spo11*$^{+/YF}$ female mice, which had mated with *Spo11*$^{+/YF}$ males were irradiated at embryonic day 15.5 (E15.5), when most oocytes are in leptotene [58,59]. These pregnant females were sacrificed to prepare spread oocyte nuclei from female embryos, 24 (E16.5) and 48 (E17.5) hours later, when the majority of oocytes that were at leptotene at the time of irradiation has reached late zygotene and pachytene, respectively (Fig. 3A). We analysed SC formation using antibodies directed against the axial/lateral element component SYCP3 and the transverse filament component SYCP1 [38]. In non-irradiated *Spo11*$^{YF/YF}$ spermatocytes and E16.5 oocytes, the degree of synapsis is variable, with some nuclei showing no synapsis, whereas others showed diverse degrees of heterologous, rather than homologous, synapsis (Fig. 3B and F). Occasionally, in spermatocytes, complete synapsis between one or two chromosomes appears to occur (Fig. 3B, arrows). On average, the degree of synapsis is more extensive in *Spo11*$^{YF/YF}$ zygotene spermatocytes compared to *Spo11*$^{YF/YF}$ zygotene oocytes isolated at E16.5 (Fig. 3B, F and J). However, *Spo11*$^{YF/YF}$ oocytes isolated at E17.5 showed more synapsis than *Spo11*$^{YF/YF}$ zygotene spermatocytes (Fig. 3D, H and J). Subsequently, we measured the total length of synapsed SC (SYCP1 positive) per nucleus in spermatocytes and oocytes after irradiation. Both in *Spo11*$^{YF/YF}$ spermatocytes and oocytes, the degree of synapsis was increased upon irradiation. In spermatocytes, the SC length was increased 1.5-fold and 2.3-fold compared to non-irradiated controls, at 48 h and 120 h after irradiation, respectively (Fig. 3B–E and J). In oocytes, the SC length was increased approximately two-fold compared to non-irradiated oocytes at 24 h after irradiation (Fig. 3F–G and J). At E17.5, the extensive heterologous synapsis in non-irradiated *Spo11*$^{YF/YF}$ oocytes obscured most of the effect of the irradiation (Fig. 3H–J). However, the number of completely synapsed axes (not entangled) was higher in irradiated compared to unirradiated *Spo11*$^{YF/YF}$ oocytes at 48 h after irradiation (Fig. 3H–I, arrows, and Fig. 3K).

2.3. Radiation-induced DSBs stimulate homologous chromosome interactions in *Spo11*$^{YF/YF}$ meiocytes

To assess whether the observed increase in synapsis formation in irradiated *Spo11*$^{YF/YF}$ meiocytes reflected increased interactions between homologous chromosomes, we performed FISH experiments using BAC probes for chromosomes 1 and 8 in irradiated and non-irradiated *Spo11*$^{YF/YF}$ spermatocytes and oocytes (Fig. 4A–D). We measured the distance between homologous (1–1, 8–8) and nonhomologous probes (1–8) (schematically shown in Fig. 4A'–D'). Subsequently, we generated plots whereby the frequencies of normalized cumulative distances between homologous and nonhomologous signals were compared between the treatment groups and also to *Spo11*$^{+/YF}$ pachytene controls. In *Spo11*$^{+/YF}$ spermatocytes, 95% of the distances between homologous probe signals were less than 6 μm, whereas this occurred only for 23% of the nonhomologous probe signals. In pachytene oocytes, homologous signals were always at less than 6 μm distance away from each other, and the distance between non-homologous sites was always more than 6 μm. (Fig. 4E and F). For untreated *Spo11*$^{YF/YF}$ spermatocytes and oocytes 30–36% of the probe distances were less than 6 μm for homologous as well as nonhomologous probes. This is to be expected, since random short distances between nonhomologous probes are expected to occur more often in a less-well organized setting of chromosomes compared to a situation in which all homologous chromosomes are properly arranged, and the homologous probes are less often in close proximity to each other. Despite the absence of an overall rescue of homologous chromosome pairing upon radiation treatment, we observed a significant difference between the homologous and nonhomologous probe distance frequency distributions in irradiated *Spo11*$^{YF/YF}$ spermatocytes at 120 h, and in irradiated *Spo11*$^{YF/YF}$ oocytes at 48 h, whereby 43% of the homologous probe distances were less than 6 μm for both (Fig. 4E,F and Supplemental Fig. 2). At these time points, nonhomologous probe signals at distances closer than 6 μm from each other were observed at clearly lower frequency (28% and 31%, for spermatocytes and oocytes, respectively). No such statistically significant differences between the distribution curves were observed at the other time points in irradiated *Spo11*$^{YF/YF}$ spermatocytes and oocytes (Supp. Fig. 2). These results indicate that irradiation with 5 Gy results in a small increase in the frequency of homologous chromosome interaction, compared to non-irradiated controls.

2.4. Repair of radiation-induced DSBs is slow in *Spo11*$^{YF/YF}$ spermatocytes and oocytes

The observed increase in homologous chromosome interactions in irradiated *Spo11*-deficient meiocytes indicated that radiation-induced DSBs might follow, at least in part, the meiosis-specific homologous recombination repair pathway. To analyse repair in more detail, we followed the dynamics of radiation-induced RAD51 foci in

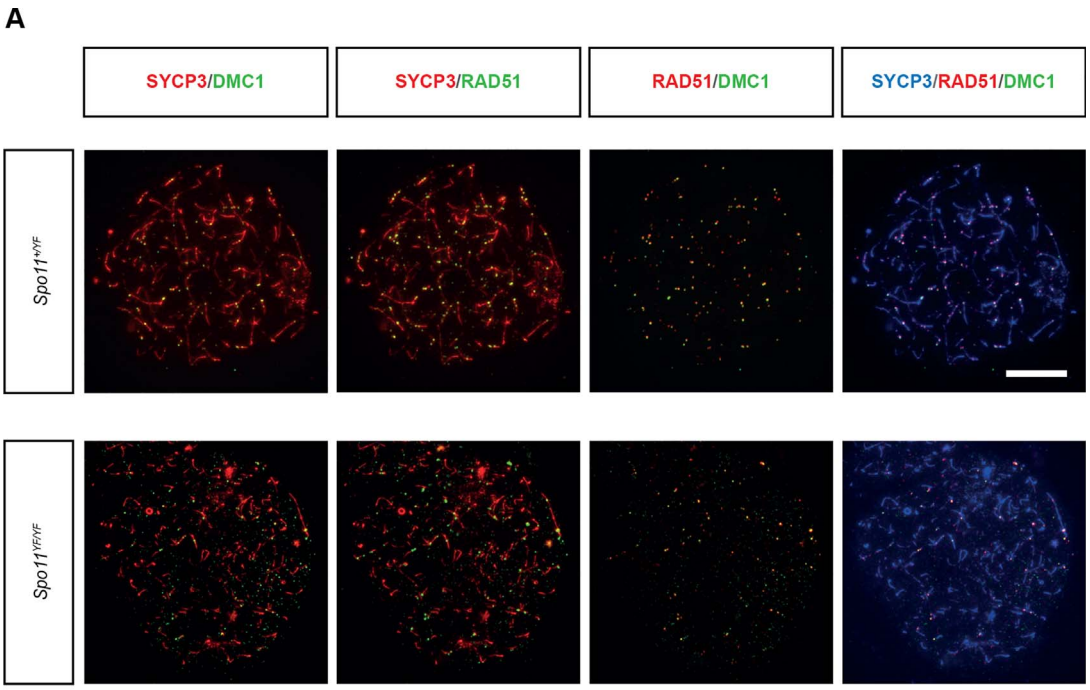

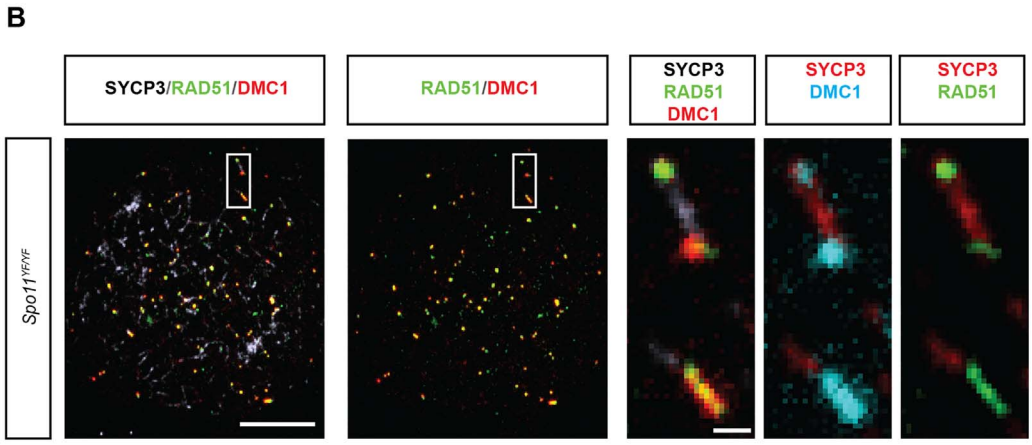

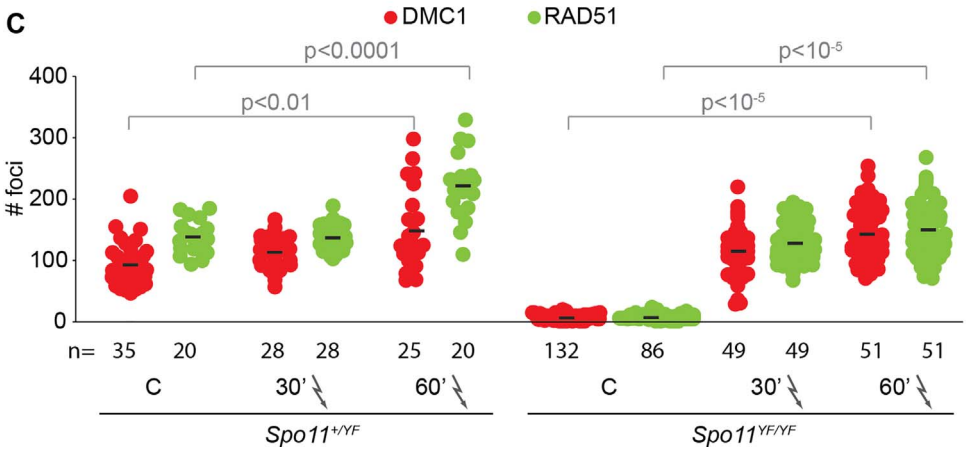

(caption on next page)

Fig. 2. RAD51 and DMC1 foci upon 5 Gy irradiation of *Spo11*$^{+/YF}$ and *Spo11*$^{YF/YF}$ spermatocytes.
(A) 5 Gy irradiated *Spo11*$^{+/YF}$ (upper panels) and *Spo11*$^{YF/YF}$ (lower panels) leptotene spermatocytes 30 min after irradiation were immunostained for RAD51, DMC1, and SYCP3. Overlayed images of the same nuclei show localization of RAD51 and DMC1 (green) to the axes (red), colocalization of RAD51 (red) and DMC1 (green) foci, and a merge of the foci with SYCP3 (blue). Scale bar represents 10 µm
(B) Triple immunostaining with anti-SYCP3, anti-RAD51, and anti-DMC1 of a *Spo11*$^{YF/YF}$ leptotene spermatocyte nucleus from a mouse that was killed 60 min after 5 Gy irradiation (confocal images). RAD51 (green) and DMC1 (red) foci localize to patches of SYCP3 (white) in the assembling axial elements. The enlarged views of a distinct area of the nucleus on the right show repair foci that are clearly recognized by both anti-RAD51 and ant-DMC1 (the majority of foci, lower part of enlargement), whereas some foci stain more strongly for RAD51, or vice versa, for DMC1 (upper part of the enlargement). Scale bar represents 10 µm in pictures of whole nuclei, and 1 µm in close-ups.
(C) The numbers of DMC1 (red), and RAD51 (green) foci were counted in *Spo11*$^{+/YF}$ and *Spo11*$^{YF/YF}$ leptotene nuclei 30 and 60 min after irradiation. Every dot represents one nucleus. Statistically significant increases in repair foci numbers are observed between non-irradiated (C) and irradiated (60′) spermatocytes of both genotypes (Mann-Whitney U). n indicates the number of analysed nuclei. (For interpretation of the references to colour in this figure legend, the reader is referred to the web version of this article.)

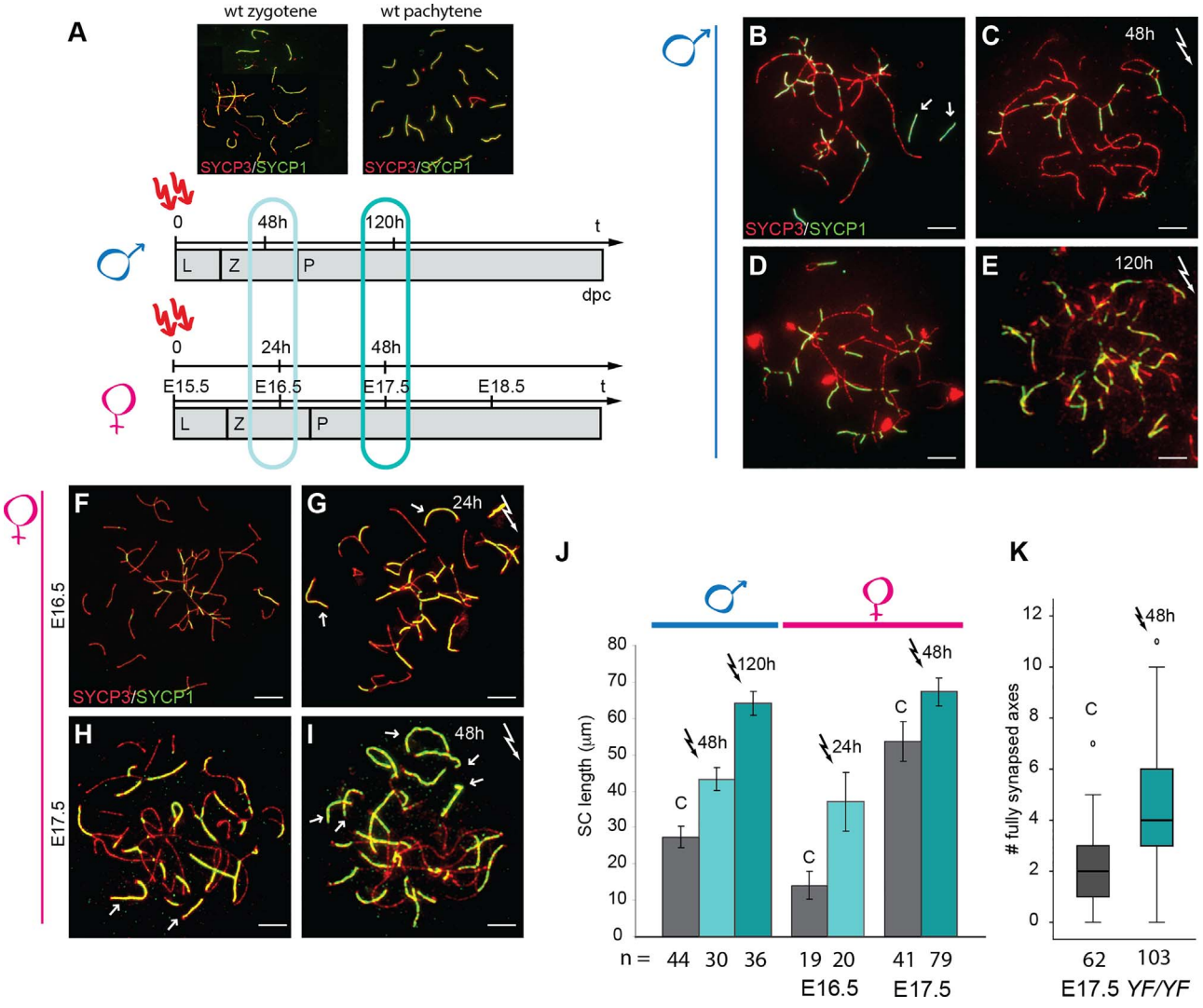

Fig. 3. Radiation-induced DSBs stimulate synapsis in *Spo11*$^{YF/YF}$ spermatocytes and oocytes.
(A) Synapsis was analysed in control and 5 Gy irradiated *Spo11*$^{+/YF}$ and *Spo11*$^{YF/YF}$ spermatocyte and oocyte nuclei. A timeline of male and female meiotic prophase in mouse is shown to indicate the correspondence between each analysed timepoint and the meiotic substage, both in spermatocytes [84] and in oocytes [58,59]. Example images of SYCP3 and SYCP1 localisation in wild type zygotene and pachytene spermatocytes are shown above the timeline. For wild type oocytes a similar pattern of SYCP3 and SYCP1 localisation accompanies prophase I, except for the fact that all chromosome pairs synapse completely in pachytene oocytes [85].
(B-I) Spread zygotene-like spermatocyte (B–E) and oocyte (F–I) nuclei of *Spo11*$^{YF/YF}$ mice, either non-irradiated (B, D, F, H), or exposed to 5 Gy irradiation (C, E, G, I). Spermatocytes were fixed at 48 h (C) or 120 h (E), and oocytes at 24 h (G) or 48 h (I) following irradiation. Synapsis was analysed via double-immunostaining for SYCP1 (green) and SYCP3 (red). Arrows indicate fully synapsed axes. Scale bars represent 10 µm.
(J) The total SC length (measured via SYCP1-signal analysis) in zygotene-like nuclei of *Spo11*$^{YF/YF}$ mice irradiated as described above was measured. Error bars indicate SEM for the indicated number of nuclei from 2 mice for each condition. C = non-irradiated controls.
(K) Boxplot showing the distribution of the number of fully synapsed (not entangled) axes in E17.5 *Spo11*$^{YF/YF}$ control (grey plot) and irradiated (turquoise plot) oocytes. Median values are indicated by the horizontal black lines within each box, which represents the middle 50% of the values. The upper and lower whiskers indicate the upper and lower quartiles of the values, respectively. Outliers are shown as small circles. $P \leq 0.0001$. Numbers of analysed nuclei are shown below the graphs (J,K), 2 animals were used for each condition.(For interpretation of the references to colour in this figure legend, the reader is referred to the web version of this article.)

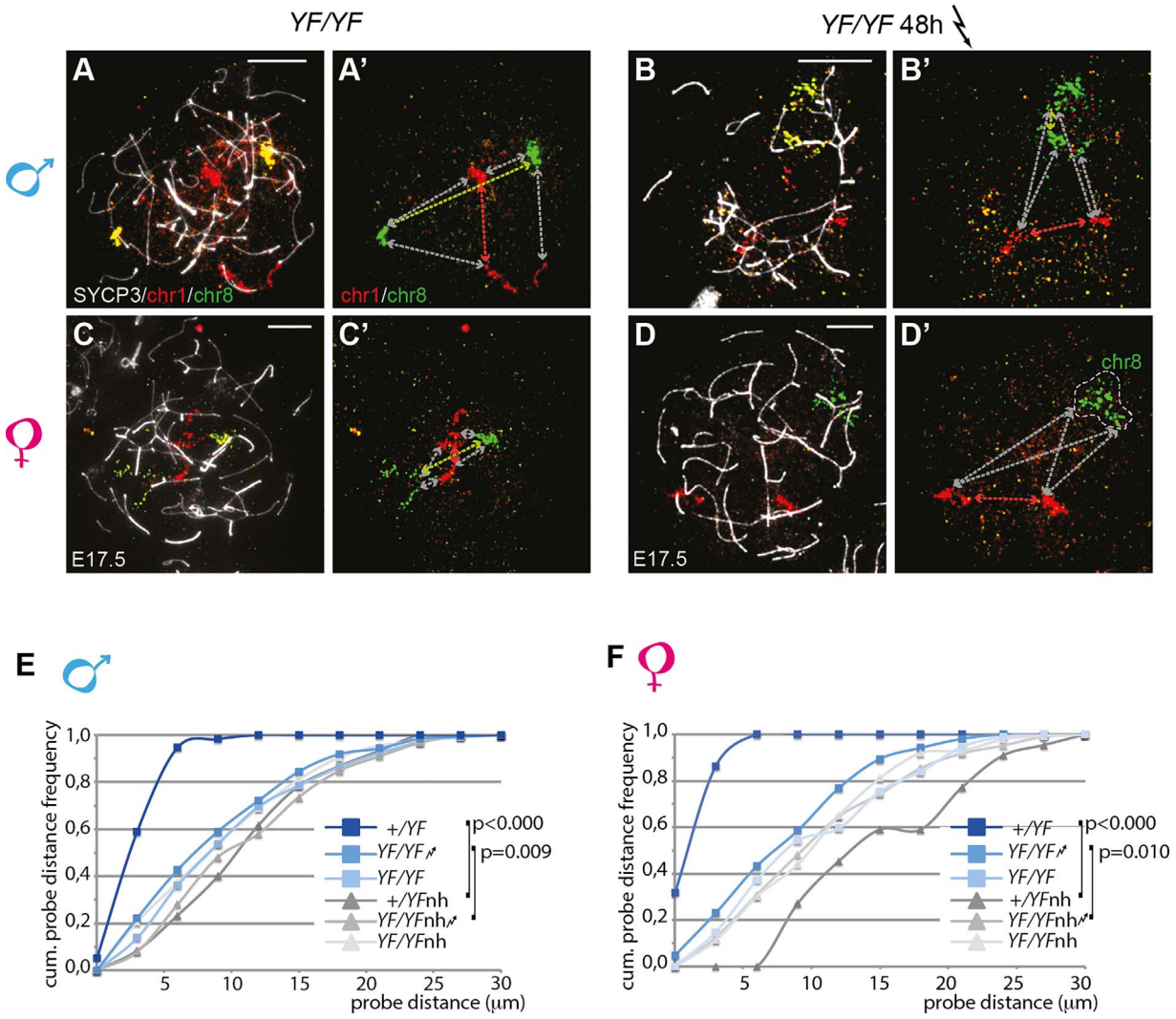

Fig. 4. Distances between homologous and nonhomologous FISH probe signals in control and 5 Gy irradiated *Spo11*$^{YF/YF}$ spermatocytes and oocytes.
(A-D) *Spo11*$^{YF/YF}$ control (YF/YF) and 5 Gy irradiated (YF/YF 48 h) spermatocytes (A, B) and oocytes (C, D) were immunostained with anti-SYCP3 (white) and subjected to FISH using BAC probes for chromosomes 1 (red) and 8 (green).
The FISH signals for chromosomes 1 and 8 are shown separately in (A'–D'). Arrows draw the minimum distance between homologous probes for chromosomes 1 (red) and 8 (green) and heterologous probes (grey, all combinations). In D' both probe signals for chromosome 8 formed a single domain inside the nucleus marked by the dashed white line. Scale bars represent 10 μm.
(E-F) Normalized cumulative frequency of probe distances in 5 Gy irradiated and non-irradiated *Spo11*$^{YF/YF}$, and non-irradiated *Spo11*$^{+/YF}$ (control) spermatocytes (E) and oocytes (F), analysed at 120 h (spermatocytes) or 48 h (oocytes) after treatment. (n = 2 animals per genotype, numbers of nuclei analysed are indicated in Supplemental Fig. 2). Blue lines indicate homologous probe distances of non-irradiated heterozygote control and irradiated (indicated by lightning symbol) and non-irradiated YF/YF samples. Grey lines indicate nonhomologous (nh) probe distances. *p*-values of significant differences (Kolgomorov-Smirnov) are indicated.(For interpretation of the references to colour in this figure legend, the reader is referred to the web version of this article.)

Table 2
Time-course of RAD51 foci in control and 5 Gy irradiated *Spo11*$^{+/YF}$ and *Spo11*$^{YF/YF}$ meiocytes (averages ± standard deviation; n > 60).

			Spo11$^{+/YF}$	*Spo11*$^{YF/YF}$
spermatocytes	zygotene	control	151 ± 26[a]	6 ± 4[a]
		48 h	162 ± 27	63 ± 14††
	mid-pachytene(-like)	control	40 ± 19[a]	6 ± 4
		120 h	41 ± 19	47 ± 12††
oocytes	E16.5	control	129 ± 35[a]	5 ± 4[a]
		24 h	156 ± 45†	94 ± 16††
	E17.5	control	41 ± 23[a]	43 ± 35[a]
		48 h	59 ± 24†	112 ± 24††

†,††Significantly different from non irradiated control of the same genotype (†p ≤ 0.05; ††p < 0.001, Mann–Whitney U).
[a] data from [42].

spermatocytes and in oocytes at the above-mentioned timepoints following irradiation (see also Fig. 3A), selecting nuclei of the appropriate stage, as described in the Materials and Methods section. In adult *Spo11*$^{YF/YF}$ mice, the population of meiotic cells will include different stages, thus also zygotene and pachytene-like spermatocytes will be hit at the moment of irradiation. However, these cells are expected to progress to different stages than those that were analysed, or would be eliminated by apoptosis, and are therefore not represented in this analysis. Interestingly, the absolute number of foci did not significantly differ between irradiated and non-irradiated *Spo11*$^{+/YF}$ spermatocytes at the 48 and 120 h timepoints after irradiation (Table 2). However, this was not the case for irradiated *Spo11*$^{YF/YF}$ zygotene- and pachytene-like spermatocytes, which had much more abundant foci than non-irradiated matched controls. (Table 2, Fig. 5 A–D). In *Spo11*$^{+/YF}$ oocytes, foci numbers were still significantly different between irradiated and non irradiated nuclei, both at 24 and 48 h after irradiation, but the

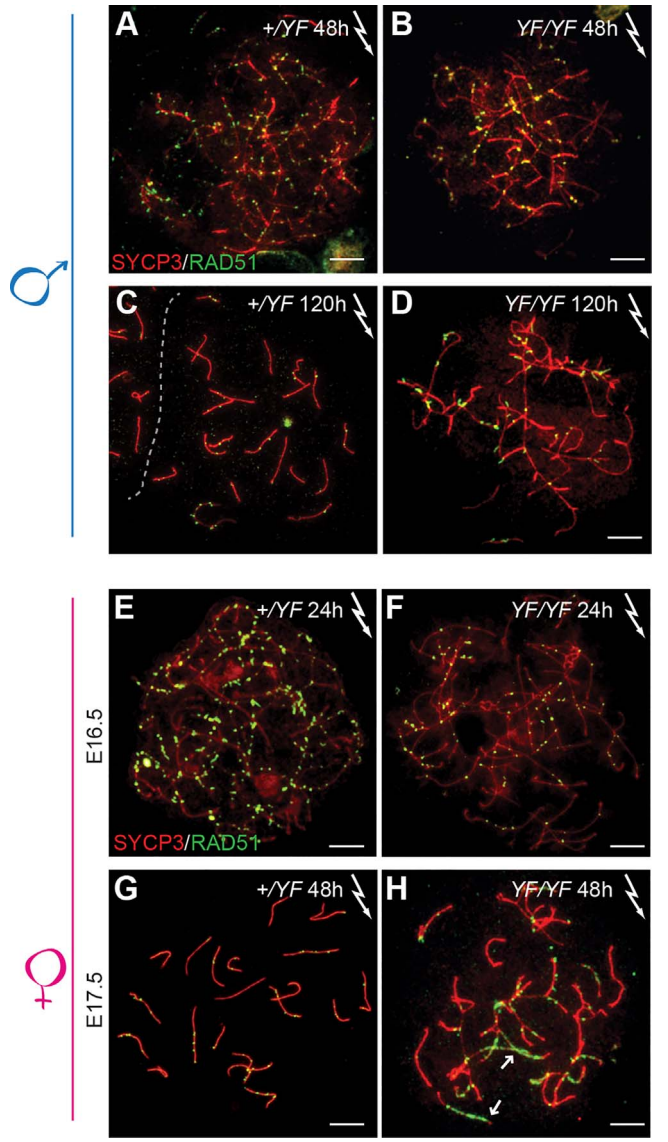

Fig. 5. Repair dynamics of radiation-induced DSBs in *Spo11*$^{+/YF}$ and *Spo11*$^{YF/YF}$ spermatocytes and oocytes (A–H) 5 Gy irradiated spermatocytes (A–D) and oocytes (E–H) from *Spo11*$^{+/YF}$ (A, C, E, G) and *Spo11*$^{YF/YF}$ (B, D, F, H) mice, immunostained for RAD51 (green) and SYCP3 (red). Size bars represent 10 μm. (For interpretation of the references to colour in this figure legend, the reader is referred to the web version of this article.)
(A–D) Spermatocytes were collected 48 (A, B) and 120 (C,D) hours after 5 Gy irradiation, to analyse late zygotene and pachytene-like stages, respectively.
(E–H) Oocytes were collected 24 h (E16.5) (E,F) and 48 (E17.5) (G,H) hours post 5 Gy irradiation, to analyse late zygotene and pachytene-like stages, respectively.

differences were relatively small, in particular at the 48 h time point, in the pachytene-like nuclei. (Table 2, Fig. 5E–H). In contrast, there was a more than two-fold difference between irradiated and non-irradiated pachytene-like oocytes of *Spo11*$^{YF/YF}$ mice. Thus, we conclude that irradiation-induced DNA breaks can be repaired efficiently when SPO11-induced DNA breaks ensure correct homolog pairing and synapsis, but not in the absence of SPO11-induced breaks, in association with asynapsis.

2.5. Faster turnover of radiation-induced RAD51 and DMC1 foci in spermatocytes on a Hormad1$^{-/-}$ background

HORMAD1 is one of the two mammalian homologs of the yeast Hop1 protein [25,60,61]. In yeast it has been shown that this protein is part of the machinery that mediates the interhomolog bias [19,62–64]. HORMAD1 localizes to axial elements, and is partially depleted from axial elements upon synapsis initiation. In the absence of HORMAD1, fewer DSBs are induced, and synapsis is incomplete [45,65,66]. In addition to its role in meiotic DSB formation, repair and synapsis, HORMAD1 is also involved in checkpoint regulation [45,65]. The published data are also consistent with the possibility that HORMAD1 inhibits completion of DSB repair along unsynapsed axial elements [25,44,45]. Such an inhibitory function would prevent completion of DSB repair until homologous pairing and synaptonemal complex formation is sufficiently established. Then, after synaptonemal complex-induced HORMAD1 depletion, repair would be rapidly achieved. Given this hypothesis, we speculated that removal of HORMAD1 might allow faster repair of exogeneous DSBs in meiocytes. To explore this, we analysed exogenous DSB foci in spermatocytes of *Spo11*$^{-/-}$/*Hormad*$^{-/-}$ double knockout mice, in comparison to *Spo11*$^{-/-}$ mice. Here we did not aim to rescue chromosome pairing but only wished to analyse the dynamics of processing of the DSBs. Thus, we chose to irradiate mice with 3 Gy, in order to reduce possible secondary effects of the radiation as much as possible. In addition, we performed 5-ethynyl-2′-deoxyuridine (EdU) injections to label the premeiotic S-phase 24 h prior to the irradiation, because we wanted to unequivocally identify a cohort of cells, independent of functional markers of prophase progression, such as synapsis, since HORMAD1-deficiency reduces overall synapsis [45]. At the moment of irradiation (T = 0) 65% of EdU-labelled cells were observed to be in leptotene (Fig. 6A; preleptotene, 25%; early zygotene, 10%; n = 100). DSB repair foci were counted in EdU-labelled nuclei at T = 1 h, T = 24 h and T = 48 h in 2 mice of each genotype. First, we analysed whether DSB repair foci still accumulated on the chromosomal axes, and observed that this process is apparently independent of HORMAD1 (Fig. 6B, Supplemental Fig. 3A, B). Then we analysed the number of RAD51 foci at all the different time points (Fig. 6B–D). It is clear that in this experimental setting, turnover of foci appears to be slower compared to the previous experiment, since around 40% of the 144 radiation-induced RAD51 foci were still present in 5 Gy irradiated *Spo11*$^{yf/yf}$ zygotene nuclei at 48 h after irradiation (Table 2), whereas 80% of the 49 radiation-induced foci were still observed in zygotene nuclei 48 h after 3 Gy irradiation of *Spo11*$^{-/-}$ leptotene spermatocytes (Fig. 6C and D, Table 3).

The absolute numbers of induced foci cannot be compared between the two experiments, because we used a slightly different counting method (see materials and methods). However, within this experiment, we clearly observed that fewer foci remain at both 24 h and 48 h after irradiation in the *Spo11*$^{-/-}$/*Hormad*$^{-/-}$ double knockout spermatocytes, compared to *Spo11*$^{-/-}$ spermatocytes at each of these time points (Fig. 6C and D, Table 3). Next, we also analysed DMC1 foci and observed a similar effect, although it was less clear, possibly due to a less efficient detection of DMC1 relative to RAD51 (Fig. 6E, Supplemental Fig. 3C–E, Table 3). To make sure that the reduction in DSB foci numbers was not due to premature loss of DMC1 and RAD51 from ssDNA, we also analysed RPA foci numbers, both at 1 h and 48 h after irradiation, in both genotypes. Here we observed similar numbers of foci at both time points (Fig. 6F and G, Table 3). In general, RPA will bind to the 3′ ssDNA overhangs of processed DSBs that are not bound by recombinases, or to ssDNA that forms during D-loop formation associated with strand invasion when repair progresses. Therefore, these RPA foci numbers are difficult to interpret in terms of repair progression. We conclude that HORMAD1 deficiency increases the turnover of RAD51/DMC1 marked recombination intermediates, which might be indicative of faster repair kinetics.

3. Discussion

3.1. Radiation-induced DSB repair foci are tethered to the axial elements shortly after induction and contain both RAD51 and DMC1

In yeast, SPO11-induced breaks are most likely formed on the axes

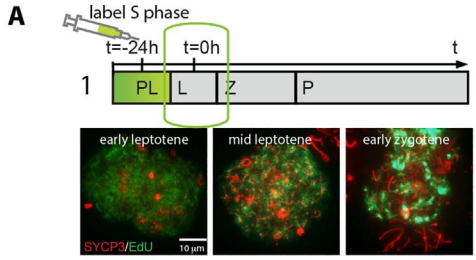

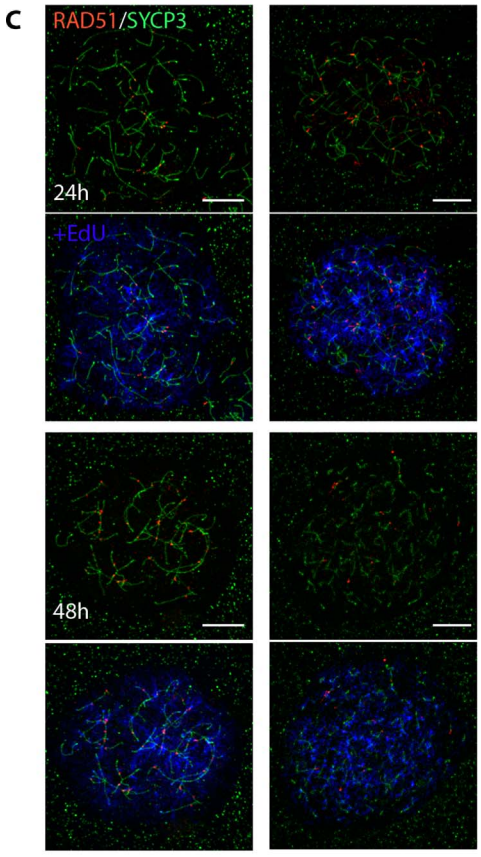

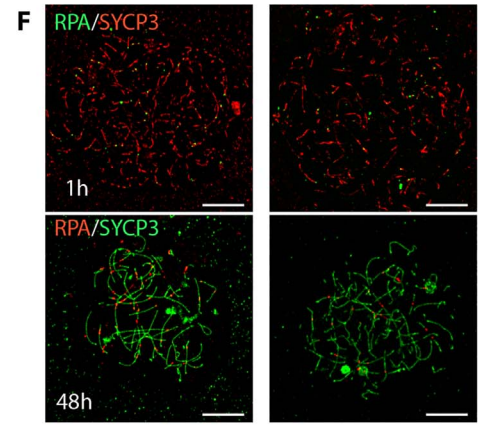

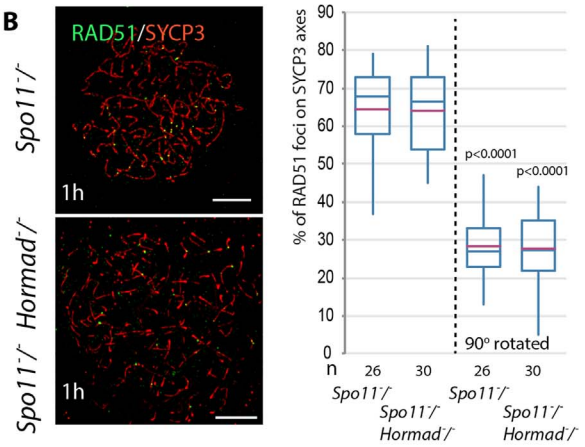

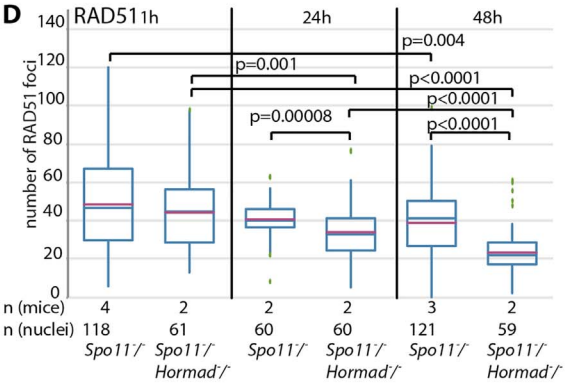

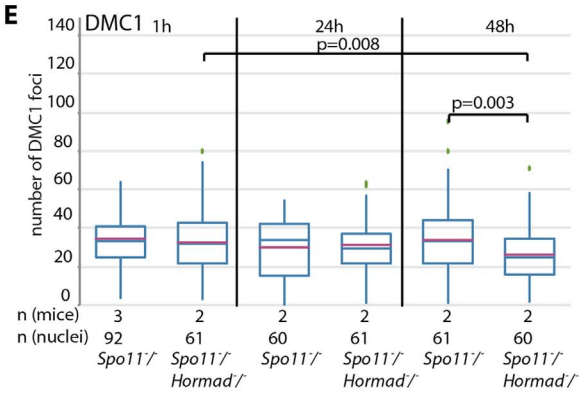

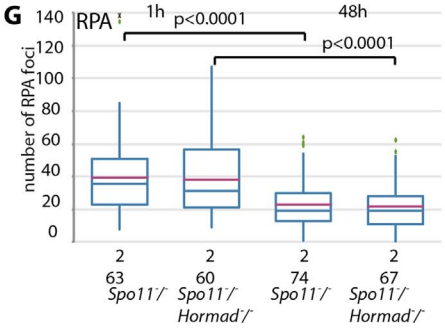

(caption on next page)

Fig. 6. Faster disappearance of radiation-induced DSB repair foci in the absence of HORMAD1.
A) EdU-labeling of a cohort of preleptotene cells 24 h prior to irradiation. At t = –24 h EdU will be incorporated in cells undergoing S-phase. At T = 0 h we assessed the stages of the EdU-positive cells by performing immunostaining on spermatocyte spread nuclei for SYCP3 (red) in combination with the click-reaction for EdU (green). Examples of labelled cells are shown.
B) Left: 3 Gy irradiated *Spo11*$^{-/-}$ (top panels) and *Spo11*$^{-/-}$/*Hormad1*$^{-/-}$ (lower panels) spermatocytes at 1 h following irradiation were immunostained for RAD51 and SYCP3, right: Quantification (boxplots) shows percentages of RAD51 foci colocalising with SYCP3 in *Spo11*$^{-/-}$ and *Spo11*$^{-/-}$/*Hormad1*$^{-/-}$ leptotene spermatocytes, at 60 min after irradiation. n indicates the number of nuclei analysed (2 animals per genotype). Statistically significant differences between true and rotated images are marked in the plot (Mann-Whitney U). Median values are indicated by the horizontal blue lines within each box, which represents the middle 50% of the values, mean values are shown in red. The upper and lower whiskers indicate the upper and lower quartiles of the values, respectively.
C) 3 Gy irradiated *Spo11*$^{-/-}$ (left panels) and *Spo11*$^{-/-}$/*Hormad1*$^{-/-}$ (right panels) spermatocytes at 24 h, and 48 h time points following irradiation were immunostained for RAD51 and SYCP3, in combination with EdU detection. Scale bar represents 10 μm.
D) Boxplots showing quantification of RAD51 foci in 3 Gy irradiated *Spo11*$^{-/-}$ and *Spo11*$^{-/-}$/*Hormad1*$^{-/-}$ leptotene (1 h after irradiation) and EdU-positive spermatocytes (24 and 48 h after irradiation). Significant differences are indicated with *p*-values (Mann Whitney U).
E) Boxplots showing quantification of DMC1 foci in 3 Gy irradiated *Spo11*$^{-/-}$ and *Spo11*$^{-/-}$/*Hormad1*$^{-/-}$ leptotene (1 h after irradiation) and EdU-positive spermatocytes (24 and 48 h after irradiation). Significant differences are indicated with *p*-values (Mann Whitney U).
F) 3 Gy irradiated *Spo11*$^{-/-}$ (left panels) and *Spo11*$^{-/-}$/*Hormad1*$^{-/-}$ (right panels) spermatocytes at 1 h and 48 h time points following irradiation were immunostained for RPA and SYCP3. Colours are swapped at 48 h because this was a costaining with Edu. The nuclei that are shown were also positive for EdU. Scale bar represents 10 μm.
G) Boxplots showing quantification of RPA foci in 3 Gy irradiated *Spo11*$^{-/-}$ and *Spo11*$^{-/-}$/*Hormad1*$^{-/-}$ leptotene (1 h after irradiation) and EdU-positive spermatocytes (48 h after irradiation). Significant differences are indicated with *p*-values (Mann Whitney U). (For interpretation of the references to colour in this figure legend, the reader is referred to the web version of this article.)

Table 3
Time-course of DSB repair foci in 3 Gy irradiated *Spo11*$^{-/-}$ *Spo11*$^{-/-}$/*Hormad1*$^{-/-}$ spermatocytes (averages ± standard deviation; n > 60).

genotype	*Spo11*$^{-/-}$			*Spo11*$^{-/-}$/*Hormad1*$^{-/-}$		
time after irradiation	1 h	24 h	48 h	1 h	24 h	48 h
RAD51	48 ± 25	41 ± 10	38 ± 18	44 ± 19	34 ± 14	23 ± 13
DMC1	34 ± 12	30 ± 15	34 ± 19	32 ± 16	31 ± 21	26 ± 14
RPA	40 ± 25		22 ± 13	38 ± 21		22 ± 14

through an interaction with the DSB machinery components Mer2/Rec114/Mei4 [67]. In mouse, the Mei4 ortholog MEI4 is also required for SPO11-mediated induction of DSBs, and also localizes on axes before and at the time of DSB formation [27]. More recently, the HORMAD1-interacting protein IHO1 was described to act upstream of MEI4, also performing an essential role in DSB formation, most likely via promoting the formation of MEI4-containing recombinosomes [26]. The present immunocytochemical analysis of RPA, RAD51, and DMC1 foci shortly after irradiation, shows that radiation-induced DSBs are rapidly recruited to the axes in leptotene, coherent with our previous observations in irradiated wild type pachytene spermatocytes [54]. It is thus possible that a specific mechanism is responsible for recognizing radiation-induced DSBs and tethering them to the chromosome axis. It will be of interest to assess whether the damage-induced DSBs are not only colocalizing with repair proteins, but also with components of the protein complex that normally facilitates the formation of SPO11/TOPOVIBL-induced DSBs. Here we observed that tethering to the chromosomal axes is independent of HORMAD1. Together with the accumulation of DMC1 in addition to RAD51, these data indicate that the radiation-induced DSBs may be further processed in a manner similar to SPO11/TOPOVIBL-induced DSBs.

3.2. Repair of exogenous DSBs stimulates chromosome synapsis and favours homologous pairing

In mouse, lack of SPO11-induced DSBs results in loss of homologous chromosome pairing and extensive heterologous synapsis [1,3,42]. Various DNA damaging agents have been used previously to induce meiotic recombination in *Spo11* mutants in different species. It was shown that cisplatin treatment, which induces DSBs, had an effect on centromeric interactions in *Spo11* knockout spermatocytes [3]. Moreover, in yeast, fungi and worms, radiation-induced DSBs can partially or completely rescue the *spo11* mutant phenotype [43]; [68–71].

Similarly to what has been found for the species described above, the induction of DSBs via γ-radiation in *Spo11*$^{YF/YF}$ mouse meiocytes, would be expected to contribute to homologous chromosome pairing and synapsis. Indeed, we observed a clear increase in the degree of synapsis and homologous chromosome interactions upon irradiation, indicating that repair of exogenous DSBs improves synapsis. Rescue of homologous chromosome pairing was far from complete, and we suggest that this may be caused by the fact that irradiation may induce DSBs relatively frequently in regions of the genome that contain repetitive DNA. Homology-mediated repair at such sites may involve the homologous sequence of repetitive DNA located on a non-homologous chromosome. In this case, the homology search would still show a bias for a non-sister template, but would not guarantee interaction between homologous chromosomes. An alternative possibility is that despite loading of RAD51 and the meiosis specific DMC1 recombinase onto DNA ends at irradiation induced DNA breaks, the filaments may differ in molecular composition from those of SPO11-induced DSBs, and this may compromise stable strand invasions into homologs, which may result in more frequent inter-sister strand invasions and inefficient homolog pairing.

3.3. Kinetics of repair protein recruitment to radiation-induced breaks differ between *Spo11*$^{+/YF}$ and *Spo11*$^{YF/YF}$ spermatocytes

In somatic cells, irradiation has been reported to induce approximately 35 DSBs/Gy in G1 cells *in vitro*, with some variation in the extent of damage depending on oxygen level and DNA compaction [72–74]. In our model, we compared accumulation of recombinases at damage-induced DSBs between *Spo11*$^{+/YF}$ and *Spo11*$^{YF/YF}$ leptotene spermatocytes. At this stage of meiosis, there are no gross differences between the two genotypes in the chromatin structure in the nuclei, and the mice have similar sizes. Thus, we suggest that irradiation induces a comparable level of damage in leptotene nuclei of the *Spo11*$^{+/YF}$ and *Spo11*$^{YF/YF}$ genotypes. However, on a *Spo11*$^{+/YF}$ background, the number of radiation-induced recombinase foci was lower compared to the *Spo11*$^{YF/YF}$ background. In irradiated *Spo11*$^{+/YF}$ spermatocytes, part of the pool of DSB repair proteins is engaged in repair of SPO11-induced breaks, and the amount of one or more of the components of the whole machinery may become limiting. The dynamics of recombinase recruitment to DSBs may therefore be delayed in irradiated versus non-irradiated *Spo11*$^{+/YF}$ spermatocytes. Indeed, the accumulation of repair proteins occurred with slower kinetics in *Spo11*$^{+/YF}$ compared to *Spo11*$^{YF/YF}$ leptotene spermatocytes. In addition, as discussed above, feedback mechanisms that inhibit SPO11/TOPOVIBL acitivity in response to damage-signalling molecules may somewhat obscure accurate assessment of the numbers of radiation-induced DSB repair foci on a *Spo11*$^{+/YF}$ background. Still we observed little difference between irradiated and non-irradiated *Spo11*$^{+/YF}$ meiocytes at late time points following the treatment, indicating that few if any radiation-induced DSBs persist for more than 120 h. In contrast, on the

Spo11$^{YF/YF}$ background, a relatively large fraction of DSB foci is still present at the late time points, in cells that were irradiated at leptotene. When subjected to γ-radiation, somatic G2 cells preferably use HR, when a template to recover the missing genetic information is available [75,76]. During G2 phase, exogenous DSBs are repaired within 4–5 h, by using the sister chromatid as a DNA template which is in close proximity thanks to sister chromatid cohesion [77]. Meiotic prophase nuclei have also completed S phase, therefore the sister chromatid is available both in *Spo11*$^{+/YF}$ and in *Spo11*$^{YF/YF}$ meiocytes. We speculate that radiation induced DSBs cannot promote homolog pairing to the same extent as SPO11-induced breaks, and that inhibition of intersister repair results in inefficient repair of radiation induced DSBs in the *Spo11*$^{YF/YF}$ background. We anticipate that *Spo11*$^{YF/YF}$ as well as *Spo11*$^{+/YF}$ meiocytes have the capability of processing radiation-induced DSBs, and we envisage two distinct explanations for the higher efficiency repair of irradiation-induced DSBs on *Spo11*$^{+/YF}$ as compared to *Spo11*$^{YF/YF}$ backgrounds. First, in wild type or heterozygous nuclei, homologous synapsis is ongoing with the aid of SPO11-induced DSBs. As a consequence, the homologous chromosome will more frequently be nearby and available as a repair template for the exogenous DSBs in *Spo11*$^{+/YF}$, compared to *Spo11*$^{YF/YF}$ nuclei, perhaps allowing more rapid repair of radiation-induced DSBs that might not be able to repair from sister chromatids during meiosis. Second, DSB repair is delayed in all synaptic mutants, hence asynapsis likely represent a kinetic block to both intersister and interhomolog repair during meiosis. Therefore, effective synapsis formation in *Spo11*$^{+/YF}$, but not in *Spo11*$^{YF/YF}$, meiocytes could promote repair of irradiation induced DSBs irrespective of template choice.

3.4. Repair of radiation-induced DSBs on a SPO11-deficient background is inhibited by HORMAD1

HORMAD1 is known to stimulate synapsis. This function is at least partially independent of DSB formation, since heterologous synapsis in *Spo11*$^{-/-}$ spermatocytes is reduced in the absence of HORMAD1 [45]. In yeast, *Hop1* mutation (ortholog of *Hormad1*) reduces the interhomolog bias [19,62–64]. In mouse such a function for HORMAD1 is difficult to analyse, since DSB formation is strongly reduced in the absence of HORMAD1 [45]. Therefore, we irradiated *Spo11/Hormad1* double knockout mice to study the effect of HORMAD1 on the turnover of such exogenous DSB repair foci to provide more insight in its function during meiotic HR. This experiment was performed using a slightly different setting and method compared to the previous experiment, and if we compare the two irradiation dosages (3 Gy versus 5 Gy) we do not observe the expected proportional difference in the numbers of radiation induced foci at 1 h following damage induction. However, it should be noted that the technical and biological differences between the two experiments preclude a direct comparison of absolute foci numbers (see materials and methods for a detailed explanation).

Still, within this experiment, loss of HORMAD1 on the *Spo11*$^{-/-}$ background resulted in more rapid turnover of radiation-induced RAD51/DMC1 recombination foci in spermatocytes. The paralogue of HORMAD1, a protein called HORMAD2, is also a meiosis-specific axis-associated protein, whose recruitment to unsynapsed axes largely depends on HORMAD1 [78]. Interestingly, loss of HORMAD2 also leads to increased turnover of radiation-induced RAD51 recombination foci in *Spo11-/-* oocytes (DMC1 and RPA marked recombination foci were not analysed) [79]. These findings suggest that HORMAD1 and HORMAD2 share a function in modulating DSB repair on chromosome axis during meiosis. Turnover of RPA marked recombination intermediates does not seem to be affected by loss of HORMAD1, hence it is possible that HORMAD1 and HORMAD2 merely alter the choice of pathways that are used for DSB repair without altering repair kinetics in meiocytes. However, RPA marks more advanced recombination intermediates than RAD51 and DMC1, hence the increased turnover of RAD51/DMC1 recombination foci might still indicate faster progression beyond the initial stages of recombination in the absence of HORMAD1 or HORMAD2. This interpretation of the data supports the attractive hypothesis that a HORMAD1(and HORMAD2)-dependent mechanism may inhibit specifically intersister repair, or inhibit both intersister and interhomolog repair of DSBs on unsynapsed chromosome axes. Either of these putative HORMAD1-dependent mechanisms could contribute to establishment of a bias towards interhomolog DSB repair by preventing repair of DSBs until synapsis forms, which typically occurs only if recombination-mediated repair involves invading the homolog chromosome. However, we note that this is unlikely to be the sole or the most important mechanism underlying interhomolog bias in recombination in mammals. In the absence of HORMAD1, a greatly reduced number of DSBs seem to still promote pairing and SC formation primarily between homologs [45]. Hence, interhomolog bias in meiotic recombination seems to be at least partially functional without HORMAD1.

Another possible interpretation of our data would be that in the absence of HORMAD1, (heterologous) synapsis is abolished, and this somehow facilitates repair. This is unlikely, since in *Sycp1*$^{-/-}$ knockout spermatocyes, that also lack synapsis, SPO11-induced DSBs persist [33].

Taken together, the data presented in this manuscript show that damage-induced DSBs are relocated to chromosome axes, where they are processed by the meiosis-specific HR machinery, which results in an increase in homology recognition and synapsis. Nonetheless, irradiation induced DNA breaks are unable to efficiently promote normal meiotic recombination which results in persistent DSBs on unsynapsed axes on backgrounds defective in forming SPO11-induced breaks. HORMAD1 seems to contribute to the mechanisms that prevent efficient repair of irradiation induced DNA breaks, because the turnover of exogenous DSB-induced recombination foci is increased in *Spo11*-deficient spermatocytes in the absence of HORMAD1.

4. Materials and methods

4.1. Mice

All animal experiments were approved by the local animal experiments committee DEC-Consult. All animals were housed in IVC cages under supervision of the Animal Welfare Officer. Any discomfort of animals was daily scored by the animal caretakers. No more than mild or moderate discomfort of animals was expected from the treatments, and no unexpected discomfort was observed.

Spo11 mutant mice were generated as described previously [42]. *Spo11*$^{YF/YF}$ males and age matched controls were irradiated with 5 Gy with Elekta linear accelerator from a ^{137}Cs source (Crawley). At 30 min, 1 h, 48 h, and 120 h following irradiation, male mice were sacrificed to prepare spermatocyte nuclei spread preparations for immunocytochemical and FISH analyses. Pregnant heterozygote *Spo11*$^{+/YF}$ females were also irradiated with a dose of 5 Gy at E15.5. At the timepoints 24 h and 48 h after irradiation, pregnant females were sacrificed, and embryos and ovaries were collected to prepare oocyte nuclear spreads. In a separate experiment, *Spo11*$^{-/-}$ (some mice carrying an additional heterozygote allele), and *Spo11*$^{-/-}$*/Hormad*$^{-/-}$ mice (numbers and ages as shown in Supplementary Table I) were injected with EdU (single intraperitoneal injection with 100 µl 10 mM EdU in DMSO). Each of these knockouts has been described previously (*Spo11*$^{-/-}$ [1], *Sycp3*$^{-/-}$ [32], and *Hormad1*$^{-/-}$ [45]). 24 h later, mice were irradiated with 3 Gy as described above, and subsequently killed at 1 h, 24 h, or 48 h after irradiation. Testes were collected and spermatocyte nuclei were spread as described below. Tails from each embryo were used to genotype the embryos as described [42], [1,32,45] (Table 4).

4.2. Meiotic spread nuclei preparations and immunocytochemistry

Testis and ovary tissues were processed to obtain spread nuclei for

Table 4
Mouse genotypes, ages and analyses time points.

genotype		age	timepoint after 3 Gy irradiation
Hormad1	*Spo11*		
+/−	-/-	19 wk	1 h
+/−	-/-	8 wk	1 h
+/+	-/-	19 wk	1 h
+/+	-/-	9 wk	1 h
-/-	-/-	19 wk	1 h
-/-	-/-	12 wk	1 h
+/+	-/-	9 wk	24 h
+/+	-/-	18 wk	24 h
-/-	-/-	10 wk	24 h
-/-	-/-	4 wk	24 h
+/+	-/-	12 wk	48 h
+/+	-/-	4 wk	48 h
+/+	-/-	4 wk	48 h
-/-	-/-	10 wk	48 h
-/-	-/-	10 wk	48 h

immunocytochemistry as described by [80]. Spread nuclei of spermatocytes and oocytes were stained with antibodies mentioned below. Before incubation with antibodies, slides were washed in PBS (3 × 10 min), and non-specific sites were blocked with 0.5% w/v BSA and 0.5% w/v milk powder in PBS. Primary antibodies were diluted in 10% w/v BSA in PBS, and incubations were overnight at room temperature in a humid chamber. Subsequently, slides were washed (3 × 10 min) in PBS, blocked in 10% v/v normal goat or donkey serum (Sigma) in blocking buffer (supernatant of 5% w/v milk powder in PBS centrifuged at 14,000 rpm for 10 min), and incubated with secondary antibodies in 10% normal goat or donkey serum in blocking buffer at room temperature for 2 h. Finally, slides were washed (3 × 10 min) in PBS (in the dark) and embedded in Prolong Gold with or without DAPI (Invitrogen). Fluorescent images were observed using a fluorescence microscope (Axioplan 2; Carl Zeiss) equipped with a digital camera (Coolsnap-Pro; Photometrics). Fluorescent images for all quantitative analyses were taken under identical conditions for all slides from each of the two seperate experiments, and images were analyzed using the ImageJ (Fiji) software (Rasband, W.S., ImageJ, U.S. National Institutes of Health, Bethesda, Maryland, USA [http://rsb.info.nih.gov/ij/]). To carefully analyse RAD51-DMC1 colocalisation on axial elements upon irradiation, images were taken using a LSM700 confocal laser scanning microscope (Zeiss).

To quantify to what extent repair foci localise on axial elements, images were analysed using Image J (Fiji) software (Rasband, W.S., ImageJ, U.S. National Institutes of Health, Bethesda, Maryland, USA [http://rsb.info.nih.gov/ij/]), whereby thresholds were manually set for each channel, followed by conversion of the image into a binary mask, and counting of the total number of foci using the count particles function. For each image, a 90 ° rotated image (around the center of the nucleus) was generated for the channel containing the DSB foci. Then the image containing the SYCP3 mask was overlayed with the image containing the DSB-foci, and subsequently also with the rotated image. For both results, the number of foci localizing within the SYCP3 mask was then counted. Results were expressed as% of the total number of DSB repair foci for each image.

To detect EdU incorporation, slides were washed in H2O, followed by a 30 min incubation in 100 ul Click-iT EdU reaction cocktail (Invitrogen) as described in the protocol provided by the manufacturer. Then, slides were washed in 3% BSA in PBS at room temperature. Subsequently, immunostainings were carried out as desired.

4.3. Antibodies

For primary antibodies, we used mouse monoclonal antibodies anti-phosphorylated H2AX (Upstate), and anti-DMC1 (Abcam); rabbit polyclonal antibodies anti-RAD51 [81], anti-RPA (gift from dr. Peter de Boer) anti-SYCP3, anti SYCP1, and affinity-purified rabbit polyclonal anti-Rec8 (N-terminus) (gifts from dr. C. Heyting), and anti-phosphorylated H2AX (Upstate); rat polyclonal anti-SYCP3 [82]; goat polyclonal anti-SYCP3 (R&D Systems). For secondary antibodies, we used a goat anti-rabbit IgG Alexa 405/488/546/633, goat anti-mouse Alexa IgG 350/488/546/633, goat anti-rat IgG Alexa 546, donkey anti-goat Alexa IgG 555. donkey anti-rabbit Alexa IgG 488, donkey anti-mouse Alexa IgG 647 Molecular Probes.

4.4. Selection criteria for staging mutant meiocytes

To quantify the amount of induced DSBs shortly after irradiation, repair protein foci were counted in leptotene nuclei. We only included leptotene nuclei that had short patches of synaptonemal complex already formed (1–3 µm length), which is the same stage analysed for quantification of the endogenous SPO11-dependent protein foci in heterozygous controls.

For the time-course analysis of recombination foci upon irradiation, *Spo11*$^{YF/YF}$ nuclei were selected based on the extent of synapsed areas, in order to consistently select similar meiotic stages at the analysed timepoints. Spermatocytes with a total synapsis length below 21 µm (average length of 13 µm) were selected to count foci 48 h after irradiation (early zygotene) and with a total synapsis length above 21 µm (average 24 µm) to count foci 120 h after irradiation (mid-pachytene). With the same threshold set as for the 48 h timepoint in spermatocytes, we selected zygotene-like *Spo11*$^{YF/YF}$ irradiated oocytes at E16.5 (average synapsis length 14 µm), and oocytes with synapsis extending over at least 22 µm at E17.5 (average 42 µm), to select cells that would have progressed to mid-pachytene.

To measure the increase of synapsis extent upon irradiation, we included in the quantitative analysis the nuclei that showed extensive synapsis at visual inspection, both for non-irradiated and for irradiated *Spo11*$^{YF/YF}$ meiocytes.

The same class of nuclei that were analysed for synapsis extent was used for quantification of homologous pairing frequency. Positions of the selected nuclei in the specimen were recorded. Subsequently, FISH was performed and FISH signals distances (see below) were measured in the previously selected nuclei.

In the Edu labeling experiments, leptotene spermatocytes at 1 h following irradiation were selected as in the previous experiment, but at 24 h and 48 h following irradiation, all stainings were combined with EdU visualization, and all EdU-positive nuclei that were encountered were included in the analyses.

4.5. Quantification of protein foci

Imaging of immunostained nuclei (RPA, RAD51, DMC1, SYCP1, SYCP3, γH2AX) was performed with the same exposure time for each nucleus. Foci were subsequently counted using Image J software, including the Fiji plugin. For the *Spo11*$^{YF/YF}$ mice, we used the analyze particles function and set the threshold manually, in order to include the smallest visible focus in the analysis. The average area of one focus was assessed to be 40–50 pixels, so that foci with an area larger than 100 pixels were counted as multiple foci to allow approximate quantification of foci also when they were not resolved in the analysed image. In the experiment involving *Spo11* knockouts and EdU labeling, we counted foci using the find maxima function, and set the noise tolerance manually. This method detects a comparable number of foci. However, background levels depend on the particular combinations of first and secondary antibodies, as well as on the microscope that was used for detection. Since these differ between the first and second experiment, absolute numbers of foci cannot be compared between the two experiments. Care was taken to keep these factors constant for each single experiment whereby foci numbers were compared.

4.6. FISH analyses

BAC probes were used both for chromosome 1 (RP23-82C21) and chromosome 8 (CH26-18P14). BACs were labelled with biotin (Biotin-Nick Translation Kit, Roche) and digoxigenin (DIG-Nick Translation Kit, Roche) respectively. After alcohol precipitation in the presence of mouse Cot-1 DNA and salmon sperm DNA, the labelled DNA was re-suspended in formamide. An amount of 1 µg per probe was used to perform FISH as described by Mahadevaiah et al. (2009) [83] on slides that were first immunostained with SYCP1/SYCP3 (see above). Detection of the digoxigenin-labelled probe was performed with a primary antibody sheep anti-DIG (Roche diagnosics) and a secondary rabbit anti-sheep-FITC (Jackson labs). Detection of the biotin-labelled probe was performed with a primary antibody mouse anti-BIO (Roche diagnostics) and a secondary goat anti-mouse Alexa 633 (Molecular Probes).

FISH signals were analysed in Image J software (Fiji), measuring the minimum distance between domains belonging to homologous probes (1-1, 8-8) and heterologous probes (1–8, all combinations). Due to variation in nuclear size, the measured absolute distances were normalized to the nuclear diameter as follows: the average nuclear diameter size was established to be 40 µm, and this reference size was divided by the measured diameter of each analysed nucleus. The number obtained was used as a conversion factor for the probe distances measured for the respective nucleus.

Subsequently, we generated cumulative distance distribution frequencies, whereby bins of 3 micrometer where used. The dataset of normalized homologous probe distances for all nuclei of a certain genotype and time after irradiation, was compared to the corresponding dataset of normalized nonhomologous probe distances in the same nuclei using a non-parametric Kolgomorov Smirnov test (http://www.physics.csbsju.edu/stats/KS-test.n.plot_form.html), that also generates such plots and uses the largest distance between the two cumulative graphs to determine whether two datasets are significantly different.

Conflict of interest statement

The authors declare that there are no conflicts of interest.

Funding

This work was supported by the Netherlands Organization for Scientific Research (NWO) through ALW (VIDI 864.05.003 and Open Programme 819.02.020). The funders had no role in study design, data collection and analysis, decision to publish, or preparation of the manuscript.

Acknowledgement

We thank Bernard de Massy (Université de Montpellier, France) for discussion and suggestions during the initial phase of this project.

Appendix A. Supplementary data

Supplementary data associated with this article can be found, in the online version, at https://doi.org/10.1016/j.dnarep.2018.01.007.

References

[1] F. Baudat, K. Manova, J.P. Yuen, M. Jasin, S. Keeney, Chromosome synapsis defects and sexually dimorphic meiotic progression in mice lacking spo11, Mol. Cell 6 (2000) 989–998.
[2] F. Cole, L. Kauppi, J. Lange, I. Roig, R. Wang, S. Keeney, M. Jasin, Homeostatic control of recombination is implemented progressively in mouse meiosis, Nat. Cell Biol. 14 (2012) 424–430.
[3] P.J. Romanienko, R.D. Camerini-Otero, The mouse spo11 gene is required for meiotic chromosome synapsis, Mol. Cell 6 (2000) 975–987.
[4] T. Robert, A. Nore, C. Brun, C. Maffre, B. Crimi, H.M. Bourbon, B. de Massy, The TopoVIB-like protein family is required for meiotic DNA double-strand break formation, Science 351 (2016) 943–949.
[5] W. Goedecke, M. Eijpe, H.H. Offenberg, M. van Aalderen, C. Heyting, Mre11 and Ku70 interact in somatic cells, but are differentially expressed in early meiosis, Nat. Genet. 23 (1999) 194–198.
[6] N. Bennardo, A. Cheng, N. Huang, J.M. Stark, Alternative-NHEJ is a mechanistically distinct pathway of mammalian chromosome break repair, PLoS Genet. 4 (2008) e1000110.
[7] J.M. Stark, A.J. Pierce, J. Oh, A. Pastink, M. Jasin, Genetic steps of mammalian homologous repair with distinct mutagenic consequences, Mol. Cell. Biol. 24 (2004) 9305–9316.
[8] D.S. Lim, P. Hasty, A mutation in mouse rad51 results in an early embryonic lethal that is suppressed by a mutation in p53, Mol. Cell. Biol. 16 (1996) 7133–7143.
[9] T. Tsuzuki, Y. Fujii, K. Sakumi, Y. Tominaga, K. Nakao, M. Sekiguchi, A. Matsushiro, Y. Yoshimura, T. Morita, Targeted disruption of the Rad51 gene leads to lethality in embryonic mice, Proc. Natl. Acad. Sci. U. S. A. 93 (1996) 6236–6240.
[10] V. Cloud, Y.L. Chan, J. Grubb, B. Budke, D.K. Bishop, Rad51 is an accessory factor for Dmc1-mediated joint molecule formation during meiosis, Science 337 (2012) 1222–1225.
[11] J. Dai, O. Voloshin, S. Potapova, R.D. Camerini-Otero, Meiotic knockdown and complementation reveals essential role of RAD51 in mouse spermatogenesis, Cell Rep. 18 (2017) 1383–1394.
[12] D.L. Pittman, J. Cobb, K.J. Schimenti, L.A. Wilson, D.M. Cooper, E. Brignull, M.A. Handel, J.C. Schimenti, Meiotic prophase arrest with failure of chromosome synapsis in mice deficient for Dmc1, a germline-specific RecA homolog, Mol. Cell 1 (1998) 697–705.
[13] K. Yoshida, G. Kondoh, Y. Matsuda, T. Habu, Y. Nishimune, T. Morita, The mouse RecA-like gene Dmc1 is required for homologous chromosome synapsis during meiosis, Mol. Cell 1 (1998) 707–718.
[14] M. Eijpe, C. Heyting, B. Gross, R. Jessberger, Association of mammalian SMC1 and SMC3 proteins with meiotic chromosomes and synaptonemal complexes, J. Cell Sci. 113 (2000) 673–682.
[15] M. Eijpe, H. Offenberg, R. Jessberger, E. Revenkova, C. Heyting, Meiotic cohesin REC8 marks the axial elements of rat synaptonemal complexes before cohesins SMC1beta and SMC3, J. Cell Biol. 160 (2003) 657–670.
[16] K. Ishiguro, J. Kim, S. Fujiyama-Nakamura, S. Kato, Y. Watanabe, A new meiosis-specific cohesin complex implicated in the cohesin code for homologous pairing, EMBO Rep. 12 (2011) 267–275.
[17] K. Ishiguro, J. Kim, H. Shibuya, A. Hernandez-Hernandez, A. Suzuki, T. Fukagawa, G. Shioi, H. Kiyonari, X.C. Li, J. Schimenti, C. Hoog, Y. Watanabe, Meiosis-specific cohesin mediates homolog recognition in mouse spermatocytes, Genes Dev. 28 (2014) 594–607.
[18] J. Lee, T. Hirano, RAD21L, a novel cohesin subunit implicated in linking homologous chromosomes in mammalian meiosis, J. Cell Biol. 192 (2011) 263–276.
[19] A. Schwacha, N. Kleckner, Interhomolog bias during meiotic recombination: meiotic functions promote a highly differentiated interhomolog-only pathway, Cell 90 (1997) 1123–1135.
[20] S. Hong, Y. Sung, M. Yu, M. Lee, N. Kleckner, K.P. Kim, The logic and mechanism of homologous recombination partner choice, Mol. Cell 51 (2013) 440–453.
[21] P.B. Moens, D.J. Chen, Z. Shen, N. Kolas, M. Tarsounas, H.H.Q. Heng, Rad51 immunocytology in rat and mouse spermatocytes and oocytes, Chromosoma 106 (1997) 207–215.
[22] A.W. Plug, A.H. Peters, K.S. Keegan, M.F. Hoekstra, P. de Boer, T. Ashley, Changes in protein composition of meiotic nodules during mammalian meiosis, J. Cell Sci. 111 (1998) 413–423.
[23] L. Kauppi, M. Barchi, J. Lange, F. Baudat, M. Jasin, S. Keeney, Numerical constraints and feedback control of double-strand breaks in mouse meiosis, Genes. Dev. 27 (2013) 873–886.
[24] D. Thacker, N. Mohibullah, X. Zhu, S. Keeney, Homologue engagement controls meiotic DNA break number and distribution, Nature 510 (2014) 241–246.
[25] L. Wojtasz, K. Daniel, I. Roig, E. Bolcun-Filas, H. Xu, V. Boonsanay, C.R. Eckmann, H.J. Cooke, M. Jasin, S. Keeney, M.J. McKay, A. Toth, Mouse HORMAD1 and HORMAD2, two conserved meiotic chromosomal proteins, are depleted from synapsed chromosome axes with the help of TRIP13 AAA-ATPase, PLoS Genet. 5 (2009) e1000702.
[26] M. Stanzione, M. Baumann, F. Papanikos, I. Dereli, J. Lange, A. Ramlal, D. Trankner, H. Shibuya, B. de Massy, Y. Watanabe, M. Jasin, S. Keeney, A. Toth, Meiotic DNA break formation requires the unsynapsed chromosome axis-binding protein IHO1 (CCDC36) in mice, Nat. Cell Biol. 18 (2016) 1208–1220.
[27] R. Kumar, H.M. Bourbon, B. de Massy, Functional conservation of Mei4 for meiotic DNA double-strand break formation from yeasts to mice, Genes. Dev. 24 (2010) 1266–1280.
[28] D. Kidane, A.S. Jonason, T.S. Gorton, I. Mihaylov, J. Pan, S. Keeney, D.G. de Rooij, T. Ashley, A. Keh, Y. Liu, U. Banerjee, D. Zelterman, J.B. Sweasy, DNA polymerase beta is critical for mouse meiotic synapsis, EMBO J. 29 (2010) 410–423.
[29] A.J. McNairn, V.D. Rinaldi, J.C. Schimenti, Repair of meiotic DNA breaks and homolog pairing in mouse meiosis requires a minichromosome maintenance (MCM) paralog, Genetics 205 (2017) 529–537.
[30] V.L. Cressman, D.C. Backlund, A.V. Avrutskaya, S.A. Leadon, V. Godfrey, B.H. Koller, Growth retardation, DNA repair defects, and lack of spermatogenesis in BRCA1-deficient mice, Mol. Cell. Biol. 19 (1999) 7061–7075.
[31] G.V. Petukhova, P.J. Romanienko, R.D. Camerini-Otero, The Hop2 protein has a direct role in promoting interhomolog interactions during mouse meiosis, Dev. Cell 5 (2003) 927–936.
[32] L. Yuan, J.G. Liu, J. Zhao, E. Brundell, B. Daneholt, C. Hoog, The murine SCP3 gene

is required for synaptonemal complex assembly, chromosome synapsis, and male fertility, Mol. Cell 5 (2000) 73–83.
[33] F.A. de Vries, E. de Boer, M. van den Bosch, W.M. Baarends, M. Ooms, L. Yuan, J.G. Liu, A.A. van Zeeland, C. Heyting, A. Pastink, Mouse Sycp1 functions in synaptonemal complex assembly, meiotic recombination, and XY body formation, Genes. Dev. 19 (2005) 1376–1389.
[34] E. Bolcun-Filas, E. Hall, R. Speed, M. Taggart, C. Grey, B. de Massy, R. Benavente, H.J. Cooke, Mutation of the mouse Syce1 gene disrupts synapsis and suggests a link between synaptonemal complex structural components and DNA repair, PLoS Genet. 5 (2009) e1000393.
[35] E. Bolcun-Filas, Y. Costa, R. Speed, M. Taggart, R. Benavente, D.G. De Rooij, H.J. Cooke, SYCE2 is required for synaptonemal complex assembly, double strand break repair, and homologous recombination, J. Cell Biol. 176 (2007) 741–747.
[36] Y. Costa, R. Speed, R. Ollinger, M. Alsheimer, C.A. Semple, P. Gautier, K. Maratou, I. Novak, C. Hoog, R. Benavente, H.J. Cooke, Two novel proteins recruited by synaptonemal complex protein 1 (SYCP1) are at the centre of meiosis, J. Cell Sci. 118 (2005) 2755–2762.
[37] G. Hamer, K. Gell, A. Kouznetsova, I. Novak, R. Benavente, C. Hoog, Characterization of a novel meiosis-specific protein within the central element of the synaptonemal complex, J. Cell Sci. 119 (2006) 4025–4032.
[38] R.L. Meuwissen, H.H. Offenberg, A.J. Dietrich, A. Riesewijk, M. van Iersel, C. Heyting, A coiled-coil related protein specific for synapsed regions of meiotic prophase chromosomes, EMBO J. 11 (1992) 5091–5100.
[39] F. Yang, P.J. Wang, The Mammalian synaptonemal complex: a scaffold and beyond, Genome Dyn. 5 (2009) 69–80.
[40] H.H. Offenberg, J.A. Schalk, R.L. Meuwissen, M. van Aalderen, H.A. Kester, A.J. Dietrich, C. Heyting, SCP2: a major protein component of the axial elements of synaptonemal complexes of the rat, Nucleic Acids Res. 26 (1998) 2572–2579.
[41] J.A. Schalk, A.J. Dietrich, A.C. Vink, H.H. Offenberg, M. van Aalderen, C. Heyting, Localization of SCP2 and SCP3 protein molecules within synaptonemal complexes of the rat, Chromosoma 107 (1998) 540–548.
[42] F. Carofiglio, A. Inagaki, S. de Vries, E. Wassenaar, S. Schoenmakers, C. Vermeulen, W.A. van Cappellen, E. Sleddens-Linkels, J.A. Grootegoed, H.P. Te Riele, B. de Massy, W.M. Baarends, SPO11-Independent DNA repair foci and their role in meiotic silencing, PLoS Genet. 9 (2013) e1003538.
[43] L.W. Thorne, B. Byers, Stage-specific effects of X-irradiation on yeast meiosis, Genetics 134 (1993) 29–42.
[44] Y.H. Shin, M.M. McGuire, A. Rajkovic, Mouse HORMAD1 is a meiosis i checkpoint protein that modulates DNA double- strand break repair during female meiosis, Biol. Reprod. 89 (2013) 29.
[45] K. Daniel, J. Lange, K. Hached, J. Fu, K. Anastassiadis, I. Roig, H.J. Cooke, A.F. Stewart, K. Wassmann, M. Jasin, S. Keeney, A. Toth, Meiotic homologue alignment and its quality surveillance are controlled by mouse HORMAD1, Nat. Cell Biol. 13 (2011) 599–610.
[46] M.S. Wold, D.H. Weinberg, D.M. Virshup, J.J. Li, T.J. Kelly, Identification of cellular proteins required for simian virus 40 DNA replication, J. Biol. Chem. 264 (1989) 2801–2809.
[47] W.D. Heyer, M.R. Rao, L.F. Erdile, T.J. Kelly, R.D. Kolodner, An essential Saccharomyces cerevisiae single-stranded DNA binding protein is homologous to the large subunit of human RP-A, EMBO J. 9 (1990) 2321–2329.
[48] Y. Wang, C.D. Putnam, M.F. Kane, W. Zhang, L. Edelmann, R. Russell, D.V. Carrion, L. Chin, R. Kucherlapati, R.D. Kolodner, W. Edelmann, Mutation in Rpa1 results in defective DNA double-strand break repair, chromosomal instability and cancer in mice, Nat. Genet. 37 (2005) 750–755.
[49] T. Ashley, A.P. Gaeth, L.B. Creemers, A.M. Hack, D.G. de Rooij, Correlation of meiotic events in testis sections and microspreads of mouse spermatocytes relative to the mid-pachytene checkpoint, Chromosoma 113 (2004) 126–136.
[50] J. Lange, J. Pan, F. Cole, M.P. Thelen, M. Jasin, S. Keeney, ATM controls meiotic double-strand-break formation, Nature 479 (2011) 237–240.
[51] T. Ashley, A.W. Plug, J. Xu, A.J. Solari, G. Reddy, E.I. Golub, D.C. Ward, Dynamic changes in Rad51 distribution on chromatin during meiosis in male and female vertebrates, Chromosoma 104 (1995) 19–28.
[52] A.W. Plug, J. Xu, G. Reddy, E.I. Golub, T. Ashley, Presynaptic association of Rad51 protein with selected sites in meiotic chromatin, Proc. Natl. Acad. Sci. U. S. A. 11 (1996) 5920–5924.
[53] M. Tarsounas, T. Morita, R.E. Pearlman, P.B. Moens, RAD51 and DMC1 form mixed complexes associated with mouse meiotic chromosome cores and synaptonemal complexes, J. Cell Biol. 147 (1999) 207–220.
[54] A. Inagaki, E. Sleddens-Linkels, E. Wassenaar, M. Ooms, W.A. van Cappellen, J.H. Hoeijmakers, J. Seibler, T.F. Vogt, M.K. Shin, J.A. Grootegoed, W.M. Baarends, Meiotic functions of RAD18, J. Cell Sci. 124 (2011) 2837–2850.
[55] S. Schoenmakers, E. Wassenaar, P. de Boer, J.S.E. Laven, J.A. Grootegoed, W.M. Baarends, Increased efficiency of meiotic silencing of unsynapsed chromatin in the presence of irradiation-induced extra DNA double strand breaks, Reprod. Sci. 15 (2008) 46.
[56] A. Inagaki, S. Schoenmakers, W.M. Baarends, DNA double strand break repair, chromosome synapsis and transcriptional silencing in meiosis, Epigenetics 5 (2010) 255–266.
[57] E.F. Oakberg, R.L. Diminno, X-ray sensitivity of primary spermatocytes of the mouse.int, Int. J. Radiat. Biol. 2 (1960) 196–209.
[58] M. Crone, E. Levy, H. Peters, The duration of the premeiotic DNA synthesis in mouse oocytes, Exp. Cell Res. 39 (1965) 678–688.
[59] K.A. McClellan, R. Gosden, T. Taketo, Continuous loss of oocytes throughout meiotic prophase in the normal mouse ovary, Dev. Biol. 258 (2003) 334–348.
[60] S.A. Pangas, W. Yan, M.M. Matzuk, A. Rajkovic, Restricted germ cell expression of a gene encoding a novel mammalian HORMA domain-containing protein, Gene Expr. Patterns 5 (2004) 257–263.
[61] T. Fukuda, K. Daniel, L. Wojtasz, A. Toth, C. Hoog, A novel mammalian HORMA domain-containing protein HORMAD1, preferentially associates with unsynapsed meiotic chromosomes, Exp. Cell Res. 316 (2009) 158–171.
[62] J.A. Carballo, A.L. Johnson, S.G. Sedgwick, R.S. Cha, Phosphorylation of the axial element protein Hop1 by Mec1/Tel1 ensures meiotic interhomolog recombination, Cell 132 (2008) 758–770.
[63] H. Niu, L. Wan, B. Baumgartner, D. Schaefer, J. Loidl, N.M. Hollingsworth, Partner choice during meiosis is regulated by Hop1-promoted dimerization of Mek1, Mol. Biol. Cell 16 (2005) 5804–5818.
[64] L. Wan, T. de los Santos, C. Zhang, K. Shokat, N.M. Hollingsworth, Mek1 kinase activity functions downstream of RED1 in the regulation of meiotic double strand break repair in budding yeast, Mol. Biol. Cell 15 (2004) 11–23.
[65] H. Kogo, M. Tsutsumi, T. Ohye, H. Inagaki, T. Abe, H. Kurahashi, HORMAD1-dependent checkpoint/surveillance mechanism eliminates asynaptic oocytes, Genes Cells 17 (2012) 439–454.
[66] Y.H. Shin, Y. Choi, S.U. Erdin, S.A. Yatsenko, M. Kloc, F. Yang, P.J. Wang, M.L. Meistrich, A. Rajkovic, Hormad1 mutation disrupts synaptonemal complex formation, recombination, and chromosome segregation in mammalian meiosis, PLoS Genet. 6 (2010) e1001190.
[67] S. Panizza, M.A. Mendoza, M. Berlinger, L. Huang, A. Nicolas, K. Shirahige, F. Klein, Spo11-accessory proteins link double-strand break sites to the chromosome axis in early meiotic recombination, Cell 146 (2011) 372–383.
[68] A.F. Dernburg, K. McDonald, G. Moulder, R. Barstead, M. Dresser, A.M. Villeneuve, Meiotic recombination in C. elegans initiates by a conserved mechanism and is dispensable for homologous chromosome synapsis, Cell 94 (1998) 387–398.
[69] M. Celerin, S.T. Merino, J.E. Stone, A.M. Menzie, M.E. Zolan, Multiple roles of Spo11 in meiotic chromosome behavior, EMBO J. 19 (2000) 2739–2750.
[70] A. Storlazzi, S. Tesse, S. Gargano, F. James, N. Kleckner, D. Zickler, Meiotic double-strand breaks at the interface of chromosome movement, chromosome remodeling, and reductional division, Genes. Dev. 17 (2003) 2675–2687.
[71] F.J. Bowring, P.J. Yeadon, R.G. Stainer, D.E. Catcheside, Chromosome pairing and meiotic recombination in Neurospora crassa spo11 mutants, Curr. Genet. 50 (2006) 115–123.
[72] S. Barnard, S. Bouffler, K. Rothkamm, The shape of the radiation dose response for DNA double-strand break induction and repair, Genome Integr. 4 (2013) 1.
[73] I.G. Cowell, N.J. Sunter, P.B. Singh, C.A. Austin, B.W. Durkacz, M.J. Tilby, gammaH2AX foci form preferentially in euchromatin after ionising-radiation, PLoS One 2 (2007) e1057.
[74] R.L. Warters, B.W. Lyons, Variation in radiation-induced formation of DNA double-strand breaks as a function of chromatin structure, Radiat. Res. 130 (1992) 309–318.
[75] J.M. Hinz, N.A. Yamada, E.P. Salazar, R.S. Tebbs, L.H. Thompson, Influence of double-strand-break repair pathways on radiosensitivity throughout the cell cycle in CHO cells, DNA Repair (Amst) 4 (2005) 782–792.
[76] K. Rothkamm, I. Kruger, L.H. Thompson, M. Lobrich, Pathways of DNA double-strand break repair during the mammalian cell cycle, Mol. Cell. Biol. 23 (2003) 5706–5715.
[77] J. Saha, M. Wang, F.A. Cucinotta, Investigation of switch from ATM to ATR signaling at the sites of DNA damage induced by low and high LET radiation, DNA Repair (Amst) 12 (2013) 1143–1151.
[78] L. Wojtasz, J.M. Cloutier, M. Baumann, K. Daniel, J. Varga, J. Fu, K. Anastassiadis, A.F. Stewart, A. Remenyi, J.M. Turner, A. Toth, Meiotic DNA double-strand breaks and chromosome asynapsis in mice are monitored by distinct HORMAD2-independent and –dependent mechanisms, Genes. Dev. 26 (2012) 958–973.
[79] V.D. Rinaldi, E. Bolcun-Filas, H. Kogo, H. Kurahashi, J.C. Schimenti, The DNA damage checkpoint eliminates mouse oocytes with chromosome synapsis failure, Mol. Cell 67 (2017) 1026–1036 (e1022).
[80] A.H. Peters, A.W. Plug, M.J. van Vugt, P. de Boer, A drying-down technique for the spreading of mammalian meiocytes from the male and female germline, Chromosome Res. 5 (1997) 66–68.
[81] J. Essers, R.W. Hendriks, J. Wesoly, C.E. Beerens, B. Smit, J.H. Hoeijmakers, C. Wyman, M.L. Dronkert, R. Kanaar, Analysis of mouse Rad54 expression and its implications for homologous recombination, DNA Repair (Amst) 1 (2002) 779–793.
[82] W.M. Baarends, E. Wassenaar, J.W. Hoogerbrugge, S. Schoenmakers, Z.W. Sun, J.A. Grootegoed, Increased phosphorylation and dimethylation of XY body histones in the Hr6b-knockout mouse is associated with derepression of the X chromosome, J. Cell Sci. 120 (2007) 1841–1851.
[83] S.K. Mahadevaiah, Y. Costa, J.M. Turner, Using RNA FISH to study gene expression during mammalian meiosis, Methods Mol. Biol. 558 (2009) 433–444.
[84] E.F. Oakberg, Duration of spermatogenesis in the mouse and timing of stages of the cycle of the seminiferous epithelium, Am. J. Anat. 99 (1956) 507–516.
[85] N.K. Kolas, E. Marcon, M.A. Crackower, C. Hoog, J.M. Penninger, B. Spyropoulos, P.B. Moens, Mutant meiotic chromosome core components in mice can cause apparent sexual dimorphic endpoints at prophase or X-Y defective male-specific sterility, Chromosoma 114 (2005) 92–102.